Computer Modeling in Engineering & Sciences CMES, vol.120, no.2, pp.375-419, 2019

Simulation of Damage Evolution and Study of Multi-Fatigue Source Fracture of Steel Wire in Bridge Cables under the Action of Pre-Corrosion and Fatigue

Ying Wang[1, *] and Yuqian Zheng[1]

Abstract: A numerical simulation method for the damage evolution of high-strength steel wire in a bridge cable under the action of pre-corrosion and fatigue is presented in this paper. Based on pitting accelerated crack nucleation theory in combination with continuum mechanics, cellular automata technology (CA) and finite element (FE) analysis, the damage evolution process of steel wire under pre-corrosion and fatigue is simulated. This method automatically generates a high-strength steel wire model with initial random pitting defects, and on the basis of this model, the fatigue damage evolution process is simulated; thus, the fatigue life and fatigue performance of the corroded steel wire can be evaluated. A comparison of the numerical simulation results with the experimental results shows that this method has strong reliability and practicability in predicting the fatigue life of corroded steel wire and simulating the damage evolution process. Based on the method proposed in this paper, the fatigue life of steel wires with different degrees of corrosion under the action of different stress levels is predicted. The results show that as the degree of corrosion increases, the fatigue properties of steel wire gradually decrease, and the influence of existing pitting corrosion on fatigue life is far greater than that on mass loss. Stress concentration is the main cause of fatigue life of corroded steel wire in advance attenuation. In addition, the fracture process of steel wire with multi-fatigue sources and the effect of the number and distribution of pits on the fatigue life of steel wire are studied. The results show that, compared with a stepped pitting distribution, a planar pitting distribution has a greater impact on the damage evolution process. The fatigue life of steel wire is positively correlated with the number of pits and the angle and distance between pits.

Keywords: Steel wire, damage evolution, pre-corrosion and fatigue, multi-fatigue source fracture, cellular automata.

1 Introduction

Fatigue failure is one of the typical failure modes of corroded cables in bridges because the cables are exposed to polluted natural environments and subjected to long-term alternating loads. Corrosion fatigue failure is the brittle fracture process of metal materials subjected to periodic (cyclic) or aperiodic (random) alternating stress and a corrosion medium and is

[1] Jiangsu Key Laboratory of Engineering Mechanics, School of Civil Engineering, Southeast University, Nanjing, 211189, China.

[*] Corresponding Author: Ying Wang. Email: civil_wangying@seu.edu.cn.

essentially the result of the interaction of an electrochemical corrosion process and mechanical process. The effect of this interaction on material damage is much greater than that of the alternating stress and corrosion medium alone [Watson and Stafford (1998); Hirose and Mura (1985)]. The corrosion fatigue damage evolution process of steel wire in cables mainly includes two stages, crack initiation and crack propagation. Under the action of a corrosion environment, corrosion damage gradually accumulates in the components. When the damage reaches the critical state, a corrosion fatigue crack initiates. The corrosion crack then propagates gradually under the action of alternating stress. When the crack length reaches the critical length, the crack propagates rapidly, and the steel wire quickly breaks.

Studies show that uncorroded steel wire with an intact surface has strong anti-fatigue crack initiation ability and weak anti-crack propagation ability [Li, Song and Liu (1995)]. However, once corrosion occurs on the surface of high-strength steel wire, tiny pitting defects can become a source of crack initiation in the steel wire, and the anti-crack initiation ability of the corroded steel wire will significantly decrease [Nakamura and Suzumura (2013)]. Therefore, the establishment of an initial pit model based on a pitting accelerated crack nucleation mechanism is a key issue in studies of the fatigue life of corroded steel wire [Huang and Xu (2012)]. Researchers have established many models for pit evolution and corrosion fatigue crack nucleation under corrosion fatigue conditions and verified these models for specific materials and corrosion environments [Liao and Wei (1999); Perkins and Bache (2005)]. To simplify the complexity of the corrosion process, most studies presuppose the pit shape and assume that the evolution rate of pitting corrosion is the same in all directions, that is, the shape of the pits does not change during their evolution process. For example, Godard [Godard (2015)] believed that pits were hemispherical in shape and had the same size change rate in all directions during the evolution process. By observing the evolution of pits in an aluminum alloy in water, the equation for the change in pit depth with time was established. However, considering the randomness and complexity of the corrosion process, corrosion morphology is often not controllable, and the shapes of pits are diverse, including wide-shallow, narrow-deep, conical, spherical, ellipsoid, groove and so on, as shown in Fig. 1 [China National Standardization Management Committee (2001)]. In general, a more realistic pitting model should include a large number of random parameters related to the aspects of material, solution, electrochemistry, and mechanics. These parameters will greatly affect the geometric size and corrosion morphology of the pit. However, pitting growth models that consider the influence of these parameters on the pit remain lacking. Therefore, in addition to these empirical methods in the literature mentioned above, a calculation model that can predict the pitting growth process and reflect the pitting corrosion morphology based on the actual corrosion mechanism of pits should be proposed [Pidaparti, Palakal and Fang (2004)].

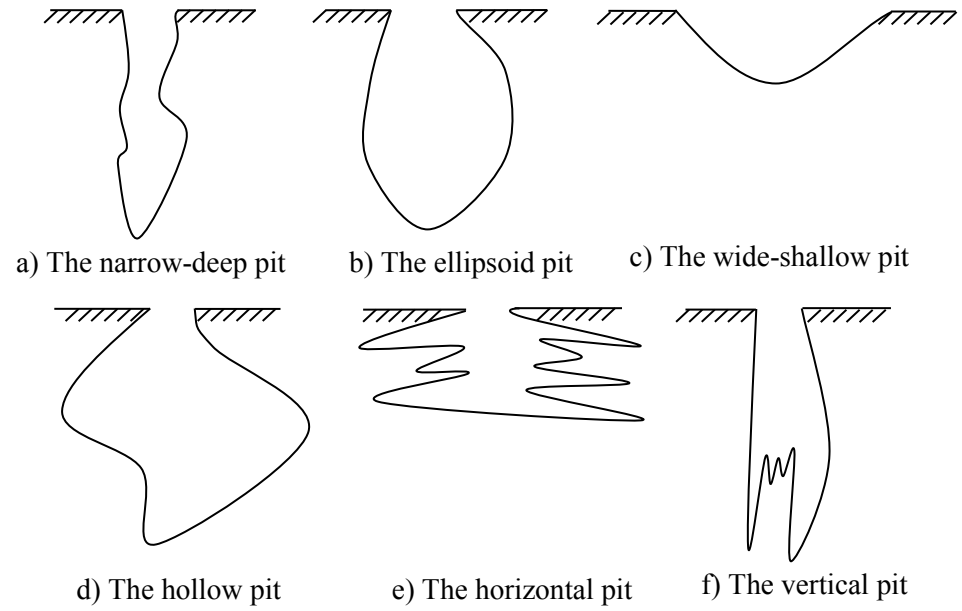

Figure 1: Morphologies of corrosion pits [China national standardization management committee (2001)]

In recent years, cellular automata (CA) technology has been gradually applied in many fields of materials science [Chowdhury, Santen and Schadschneider (2000); Wimpenny and Colasanti (1997)], especially in the field of corrosion science [DiCaprio, Vautrin and Stafiej (2011); Caprio, Vautrinul and Stafiej (2013); Stafiej, DiCaprio and Bartosik (2013)]. The CA technique is a powerful tool to describe and simulate the behavior of complex physical and chemical systems. It can simulate the system at the micro level or mesoscopic level and describe the cumulative effects on macro performance at the micro level or mesoscopic level [Wang, Song and Wang (2009)]. As an effective tool for studying complex systems, the CA method has strong universality and stability in simulating the corrosion damage evolution process [Chen and Wen (2017)]. This article therefore adopts CA technology and the practical nature of the electrochemical reaction to simulate random pitting morphology and study the fatigue damage evolution process of corroded steel wire. By defining the corrosion rules of pitting, the metal, passive film and corrosion medium are discretized into well-ordered cells in the 3-dimensional CA system. The pitting process of the metal is simulated at the mesoscopic scale, and a random initial pitting model can be automatically generated.

Previous studies have employed two main methods for damage evolution simulation: one based on the continuum damage mechanics model or one based on the fracture mechanics model [Sun (2018)]. In the damage mechanism-based method, pits are regarded as grooves, and the pitting evolution follows Faraday's law [Amiri, Arcari and Airoldi (2015)]. Based on this method, the damage distribution in a certain analysis step can be shown; however, the damage accumulation and evolution process cannot be visualized, especially the transformation between pitting and cracking. For fracture mechanic-based methods, pits are equivalent to surface cracks, and a linear superposition model [Wei (2010)] and

competition model [Austen and Mcintyre (2013)] have been established. The method based on fracture mechanics can reveal the damage evolution quantitatively, but because many factors influence the crack propagation process and the complex relationship between corrosion and fatigue, the superposition model and process competition model are not convenient for engineering applications.

To overcome the shortcomings of traditional research methods, in this paper, to explore the characteristics of fatigue damage of corroded steel wire, a material subroutine, UMAT, is written with based on the FORTRAN language, and simulations of the fatigue damage evolution of corroded material depending on the cyclic load and environmental conditions are carried out according to the life-and-death element method in ABAQUS software. Compared with the above methods, the method proposed in this paper can not only describe the distribution of fatigue damage in corroded steel wire based on the fatigue damage evolution model but also visualize the process of damage evolution based on the concept of the life-and-death element method.

The technical route for the numerical simulation method of fatigue damage evolution of corroded high-strength steel wire in bridge cables proposed in this paper is shown in Fig. 2. There is three parts in Fig. 2, including corrosion fatigue damage evolution theory, simulation of corrosion fatigue damage evolution and research on pre-corrosion fatigue life. First, for the part of corrosion fatigue damage evolution theory, based on continuum damage mechanics, a fatigue damage model suitable for corroded steel wire in a bridge cable is established, and the above model is written into a user-defined material subroutine (UMAT) using FORTRAN language. Then, for the part of simulation of corrosion fatigue damage evolution, the CA technology is utilized to generate the morphology and position of random irregular corrosion pit in MATLAB software. By using the programming interfaces between MATLAB, AutoCAD, RHINO and ABAQUS software, the data obtained by the CA method are inputted into the above software to produce the three-dimensional grid model, the surface model and the geometer model successively. Hence, the visualization of high strength steel wire with initial corrosion pit is realized. In addition, based on the linear elastic finite element method, focusing on the characteristics of fatigue damage analysis, a solution process based on cyclic block is proposed. The simulation of corrosion fatigue damage evolution is realized with reference to the concept of life-and-death element method combined with the developed UMAT. Finally, for the part of research on pre-corrosion fatigue life, the fatigue life of corroded steel wire is obtained, and the effects of the number of pits, stress level and corrosion degree on the fatigue life of steel wire are studied by using the proposed simulation method.

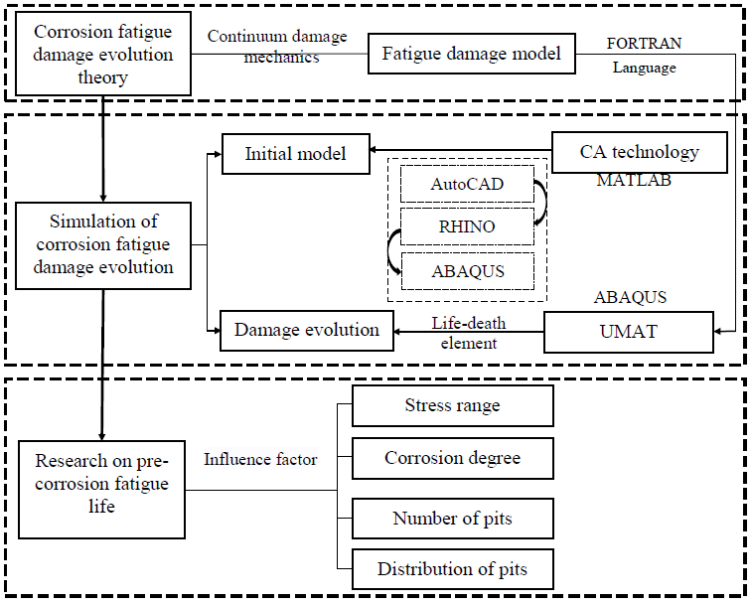

Figure 2: The technical route for the numerical simulation method of fatigue damage evolution of corroded steel wire under the action of corrosion and fatigue

2 Fatigue damage evolution model

The material damage evolution process refers to the process of performance degradation caused by the initiation, evolution and emergence of internal defects in material under external factors (alternating load, temperature change and corrosion environment, etc.) [Yu (1988)]. The pre-corrosion fatigue damage of steel wire in bridge cable includes two stages, i.e., corrosion damage and fatigue damage, which result in the formation of pits and cracks, respectively. Pitting corrosion appears before crack formation and promotes crack initiation. In this paper, the pitting evolution process is achieved by using cellular automata (CA) technology, which will be described in detail in Section 3, while the process of fatigue damage evolution is realized by using the user material subroutine UMAT, which will be described in detail in Section 4. These two processes compose the method proposed in this paper to study the fatigue damage evolution process of steel wire with corrosion damage.

In continuum damage mechanics, the macroscopic state variable D is often used to describe the distribution, characteristics and evolution process of microstructure defects [Sun (2018)]. In general, the fatigue damage variable D_f can be expressed as a function of parameters such as the stress range ΔS, maximum stress $\sigma_{\max}$, loading cyclic number N, and temperature T. The general form of the evolution equation of fatigue damage D_f can be expressed as the following [Han, Huang and Gao (2014)]:

$$\frac{dD_f}{dN} = F_f\left(\sigma_{\max}, \Delta S, D_f, T, \cdots\right) \tag{1}$$

where $F_f(\ )$ is the function to be determined. If only the influence of the cyclic stress range is considered, the fatigue damage in each cyclic load can be expressed as follows [Chaboche (1981)]:

$$F_f = (1-D)^{-\mu}\left(\frac{\Delta S}{M}\right)^B \tag{2}$$

where μ and B are parameters related to temperature, and M is material parameter related to average stress.

Based on the initial condition $N=0, D_f(0)=0$, Eq. (2) is integrated to obtain the fatigue damage evolution model:

$$D_f(N) = 1-\left[1-(\mu+1)\left(\frac{\Delta S}{M}\right)^B N\right]^{\frac{1}{\mu+1}} \tag{3}$$

Before adopting this model, the material parameters in the above model need to be fit. In this paper, the uniaxial tensile fatigue test results of high-strength steel wire specimens in Lan et al. [Lan, Xu and Ren (2017)] are used for parameter fitting, and the median S-N curve of steel wire without initial damage is written as follows:

$$\lg N_f = 23.480 - 6.649 \times \lg \Delta S \tag{4}$$

where N_f is fatigue life of steel wire.

Based on Eq. (4), the fitting values of μ, B and M are 3772.53, 6.649 and 1, respectively.

3 Modeling method of a high-strength steel wire model with an initial random defect

3.1 Simulation of the metal corrosion process based on 3D cellular automata (CA) technology

Cellular Automata, or CA for short, is a complex dynamic system that is discrete in both time and space [Li, Packard and Langton (2017)] and is mainly composed of elements such as the cell, cell state, cell space, neighbor, and discrete time set, among others. According to the definition of CA, the "cell" of its main components will have one and only one specific state, which belongs to a certain limited specified state [Langton (1984)]. According to the specific requirements, these cells are distributed on the divided cellular space grid according to a certain law, and the state of each cell changes with the time step according to the defined local rules. In other words, the state of each cell at the next moment is determined by the state at the current moment and the state of its neighbors.

The damage evolution process of metal corrosion is simulated by using the CA method. In three-dimensional cellular space, the metal/passive film/electrolyte is regarded as an automata system with a special local rule or transformation rule, which is discretized into a well-ordered cellular grid to obtain the corrosion morphology, size and distribution of pits on the metal surface.

3.1.1 Physical model

The most basic corrosion processes can be divided into three stages: 1) random diffusion of corrosive media in solution; 2) breakage of the passive film on the metal surface; 3) electrochemical reaction of the exposed metal surface in a humid environment and the metal gradually dissolves.

If the reoxidation of the metal surface in the corrosion process is not taken into account, the general formula for the basic reaction of metal dissolution in a humid environment [Pidaparti, Fang and Palakal (2008)] can be expressed as follows:

$$\mathrm{Me}+\mathrm{H_2O} \rightarrow \mathrm{MeOH_{aq}}+(1/2)\mathrm{H_2} \tag{5}$$

where Me represent metal, $\mathrm{H_2O}$ is the chemical formula of water, $\mathrm{H_2}$ is the chemical formula of hydrogen gas and $\mathrm{MeOH_{aq}}$ is the substance in solution after the reaction, which has no influence on the subsequent corrosion process and is not considered.

3.1.2 Cellular space

A discrete space is used to characterize the metal/passive film/electrolyte solution system in the CA model, and the dynamic characteristics of metal corrosion are defined by the transition rules of the cell state in discrete time. The cylindrical coordinate system is selected to describe the geometrical shape of the steel wire. The corrosion simulation accuracy is set as 0.1 mm and 3°, and thus the metal component and corrosion environment are divided into an array composed of cells. The number of cells along the three coordinate directions in the cylindrical coordinate system is represented by N_R, N_a and N_l, which are respectively 70, 120 and 140. Each cell is represented by its position coordinates of (i,j,k). A fixed boundary condition is selected; that is, a constant is selected for the cell at the boundary to simulate a finite cell space. The three-dimensional cellular space for studying the corrosion process of steel wire in a bridge cable is thus established as shown in Fig. 3.

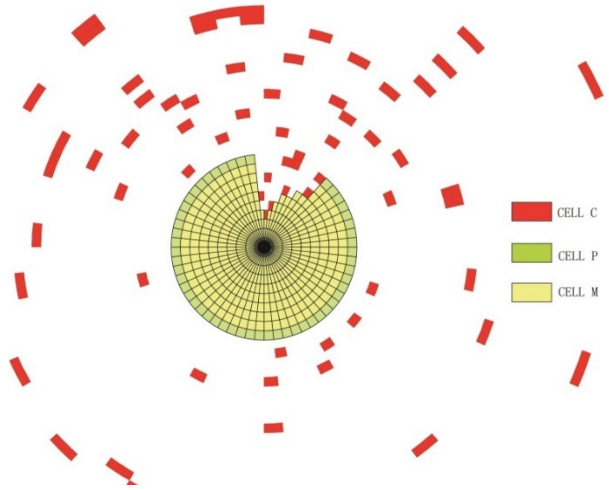

Figure 3: Cellular space for the corrosion process of steel wire

The state of each cell (i,j,k) is determined by the cell properties. As shown in Fig. 3, there are three main cellular types involved in the CA system for metal corrosion:

a) Metal cell-M: It can be corroded by the corrosive cell, and its position remains unchanged during the simulation process.

b) Passive cell-P: In the pitting evolution process, the passive film cell in the initial state will cover the outermost metal cell, and its position is basically fixed. However, in the simulation process, the passive film cell will randomly generate initial defects, and under these conditions, the passive film cell at this position will be transformed into a metal cell.

c) Corrosion cells-C: They are randomly distributed in the solution, which can corrode metal cells and move freely. In three-dimensional cellular space, the corrosion cells can randomly choose to move in a certain direction of an axis at every time step.

The initial state of the cell in each position is determined according to the size of the metal component and the concentration of corrosive solution. In this paper, the concentration of corrosive solution is set to 0.1, and the distribution of corrosion cells is stochastic uniform. That is to say, each cell out of the metal cell is given a random number that obeys uniform distribution at the interval from 0 to 1. If the number is smaller than 0.1, the corresponding cell is the corrosion cell. In addition, the location of a single initial defect is set on the middle section of steel wire.

3.1.3 Cellular transformation rules

In the cell space, the cell evolution rule is based on the most basic corrosion processes that have been mentioned in 3.1.1.

For the diffusion process in solution, within a time step, a cell C can selectively move to one of its neighbors. The neighbor type adopted in the CA model in this paper is a group of 6 neighbor cells as shown in Fig. 4. In Fig. 4, the dark cell represents the center cell, and the light cells represent the neighbor cells of the center cell. That is to say, in each time step, the corrosion cell C at position (i, j, k) spreads randomly and selectively jumps to one of its neighbor cells. If the selected neighbor cell is not occupied by other cell C or cell P, the cell C jumps to the neighbor cell; otherwise, it remains in the original position.

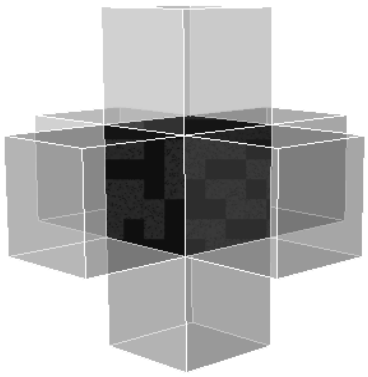

Figure 4: Cellular neighbor type

For the passive film breakage and the initial defect generation process, in the CA model, the cell P is randomly converted into a cell M, i.e.,

$$P \rightarrow M \tag{6}$$

For the metal dissolution process, in the CA model, the reaction of metal dissolution in Eq. (5) can be expressed as follows:

$$M+C \rightarrow C \tag{7}$$

which indicates that when the metal dissolves, the current position of the cell M is occupied by the cell C of the neighboring position, and then the corresponding neighboring position becomes empty.

In addition, the following space interaction is introduced to limit the random diffusion process. Within a time step, a cell C selects one of its neighbors. If the selected neighbor cell is empty or is occupied by a cell M but is chosen as a target position of another cell C, the cell C remains its original position.

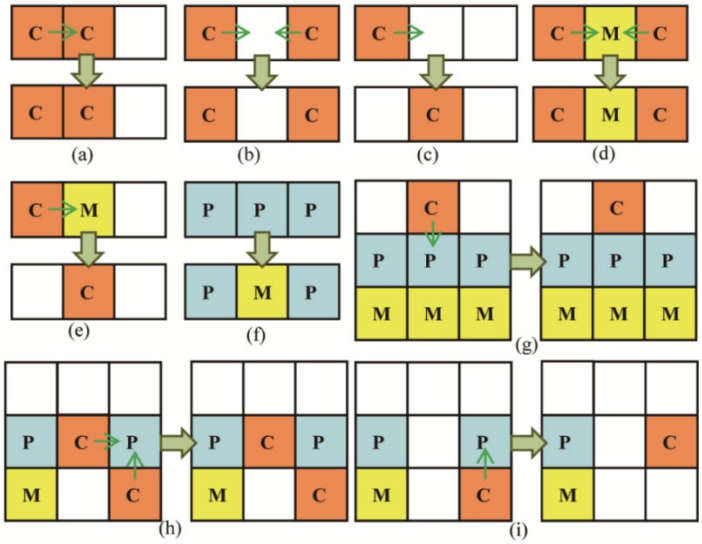

Figure 5: Cell transformation rules

Specifically, as shown in Fig. 5, the rule of cell transformation is as follows:

(1) Within a time step, cell C in initial position (i, j, k) randomly selects one of its neighbor positions and is ready to move to that position. Specifically, each cell C is given a random integer that obeys uniform distribution at the interval from 1 to 6. Each number is corresponding to one of directions, which means there is the equal-probability for all directions that cell C may move to;

(2) If the selected neighbor position in Step (1) is occupied by another cell C, then cell C remains in its initial position (i, j, k), as shown in Fig. 5(a);

(3) If the selected neighbor position in step (1) is empty but another cell C is also ready to move to this neighbor position, then cell C remains in its initial position (i, j, k), as shown in Fig. 5(b);

(4) If the selected neighbor position in Step (1) is empty and no other cell C is ready to move to this neighbor position, then the cell C moves to the neighbor position, and the original position (i) becomes empty, as shown in Fig. 5(c);

(5) If the selected neighbor position in Step (1) is occupied by a cell M but another cell C is ready to move to this neighbor position, then cell C remains in its initial position (i, j, k), as shown in Fig. 5(d);

(6) If the selected neighbor position in Step (1) is occupied by a cell M and no other cell C is ready to move to this neighbor position, then cell M disappears, cell C moves to this neighbor position, and the original position (i, j, k) becomes empty, as shown in Fig. 5(e);

(7) If a cell P breaks at this point of time, then cell P becomes a cell M, as shown in Fig. 5(f);

(8) If the selected neighbor position in Step (1) is occupied by cell P and cell C is located outside the metal space, then cell C remains in its initial position (i, j, k), as shown in Fig. 5(g);

(9) If the selected neighbor position in Step (1) is occupied by cell P and cell C is located inside the metal space but another cell C is also ready to move to this neighbor position, then cell C remains in its initial position (i, j, k), as shown in Fig. 5(h);

(10) If the selected neighbor position in Step (1) is occupied by cell P and cell C is located inside the metal space and no other cell C is ready to move to this position, then cell P disappears, cell C moves to a neighbor position, and the original position (i, j, k) becomes empty, as shown in Fig. 5(i).

3.2 Establishment of a three-dimensional model of the pit

To study the properties of corroded steel wire, a three-dimensional model of corroded wire must be established to further simulate the fatigue damage evolution of steel wire and predict its fatigue life. The corrosion morphology of a steel wire surface is simulated based on the data generated in the CA model. First, considering the irregularity and discretization of the generated data, the function of griddata() in MATLAB software is used for data interpolation in this paper, and the interpolation method is cubic based on a triangle.

To import the fitted surface into AutoCAD software, a transformation program, mat2cad, is written in this paper, based on the principle of AutoCAD software drawing. That is, the AutoCAD drawing is completed through the grid (the same principle as in MATLAB). Therefore, as long as the coordinates of all points in a graph are generated, it can be imported into AutoCAD software.

The data generated in MATLAB software by CA method are imported one by one into AutoCAD software, Rhino software and ABAQUS software to generate a three-dimensional grid model, the surface model and the geometry model successively. The object of the whole process is to easily realize the visualization and substantialization of the corrosion pit generated by CA method. Specifically, the grid model is generated directly by data transmission between MATLAB software and ABAQUS software. Then, the grid model is inputted into Rhino software to generate the surface model that is irregular but smooth by a plugin, namely, RhinoResurf plugin. And a 3D solid model is generated in Rhino software directly by using the function of automatic solid generation. Finally, the 3D solid model is inputted into ABAQUS software to generate 3D geometry model used

for damage evolution simulation. The reason for complex data transition between four softwares, rather than directly transition from MATLAB software to ABAQUS software, is that the data produced by CA model in MATLAB software is too complex to fit the surface model directly. The plug-in in Rhino software can solve the problem perfectly, and the 3D solid model is created easily in Rhino software. The generation process is shown in Fig. 6. The generated model is based on the mechanism of metal anodic dissolution and can reasonably describe the irregular morphology and distribution of pits in line with the actual situation.

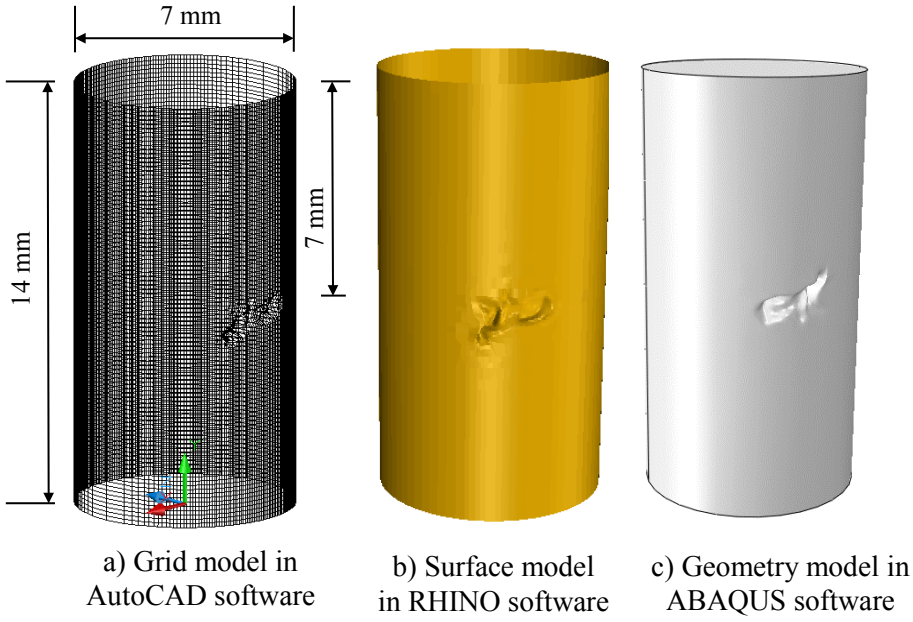

Figure 6: Generation process of 3-dimensional geometry model of high-strength steel wire with corrosion pit

The termination condition of cellular transformation in CA model is that the mass loss rate of steel wire reaches 0.25%.

4 Simulation of the damage evolution of steel wire

4.1 Structure solving process based on a cyclic block

An actual loading cycle corresponds to the process in which the load increases from the minimum to the maximum and then decreases to the minimum. Due to the high number of cycles, it is difficult to analyze each cycle. For high-strength steel wire with high fatigue life, the material damage will change obviously only when the loading numbers are large; therefore, it is not necessary to calculate the damage during each loading cycle [Han, Huang and Gao (2014)].The cyclic block is used to represent a certain loading number and is defined as the calculation accuracy; that is, the damage value of the material remains unchanged in each cyclic block. When the analysis is carried out to the next cyclic block, the damage value of the material will be updated according to the state of the last cyclic

block at the end of loading. However, the solution process of ABAQUS software is based on the analysis step, and each analysis step corresponds to the analysis of a loading or unloading process. Therefore, in this paper, each cycle block is composed of a loading analysis step or a unloading analysis step in ABAQUS. In the loading analysis step, the load increases from the minimum to the maximum, while in the unloading analysis step, the load decreases from the maximum to the minimum. In short, the relationship among the loading number, cyclic block, calculation accuracy and analysis step can be expressed as follows:

$$N_{cb} = \mathrm{INT}\left(\frac{N_T}{n}\right) \tag{8}$$

$$N_{cb} = \left(N_{as} + 1\right)/2 \quad \text{if } N_{as} \text{ is odd} \tag{9}$$

$$N_{cb} = N_{as}/2 \quad \text{if } N_{as} \text{ is even} \tag{10}$$

where, N_{cb} is the number of cyclic blocks, N_T is the total number of cyclic loads, n is computational accuracy, N_{as} is analysis step and INT( ) is the integral function. Therefore, the relationship between the cyclic block, the analysis step and the number of cyclic loads is as shown in Fig. 7.

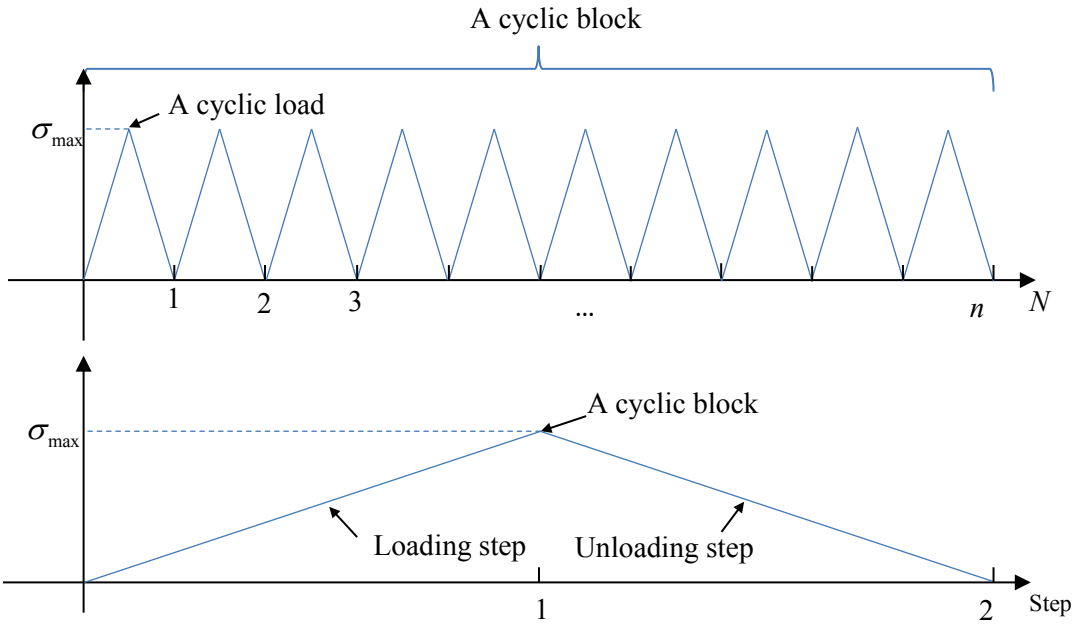

Figure 7: Relationship between the cyclic block, the computational accuracy, the analysis step and the number of cyclic loads

The material damage evolution model adopted in this paper reflects the relationship among the material damage, loading number, and stress range. In the process of damage evolution analysis, the damage is mainly related to the cyclic block, and it can be theoretically

considered that the damage accumulation only occurs at the discrete time point at the end of the cycle. In other words, when the analysis step is 1, the initial material characteristics are used to calculate the structural response, and then the accumulated damage value is calculated. For the subsequent loading analysis step, namely, the process in which the cyclic load increases from the minimum to the maximum, before calculating the structural response in this cycle, the damage accumulation increment is first calculated according to the structural response of the previous cycle. Then, the calculated damage accumulation increment is added to the total damage. Finally, according to the total damage, the structural response of this cycle is calculated by updating the material characteristics. Therefore, at the p^{th} cycle, the total damage value D_p of the structure can be expressed as follows:

$$D_p = D_{p-1} + \Delta D_P \tag{11}$$

where D_p and D_{p-1} refer to the total damage values in the p cycles and (p-1) cycles, respectively, and ΔD_P refers to the damage accumulation increment caused by the $(p-1)^{th}$ cycle and is calculated as follows:

$$\Delta D_p = D_{f/cf}(\Delta\sigma_{p\text{-}1}, (p-1)\cdot n, \cdots) - D_{f/cf}(\Delta\sigma_{p\text{-}1}, (p-2)\cdot n, \cdots) \tag{12}$$

where $D_{f/cf}()$ is the material damage evolution model used in this paper, $\Delta\sigma_{p\text{-}1}$ is the stress range during the $(p-1)^{th}$ cycle, p is the cyclic block, and n is the calculation accuracy.

If the damage value D of an element in the cyclic block is greater than a value close to 1, it is judged that the element has failed. Under these circumstance, the stiffness matrix of the element is multiplied by (1-D) because the deactivated degrees of freedom in the "dead" element need to be restrained to reduce the number of solving equations and prevent error. According to the reference [Lan, Xu and Liu (2018)], the value close to 1 in this paper is set as 0.9.

For the entire analysis, during each load cycle the material has accumulated the damage caused by the previous cycle, which requires the solution process of each seemingly independent cyclic block to be connected. Consequently, the impact of damage related to the loading number on the subsequent analysis should be considered. In this paper, a solution process suitable for corrosion-fatigue damage analysis of steel wire is established by referring to the analysis process of general nonlinear materials.

4.2 Implementation of the material subroutine

The user-defined material subroutine (UMAT) is a FORTRAN programming interface provided by ABAQUS for users to customize material properties, thereby allowing users to use the undefined material model in the ABAQUS material database. ABAQUS is able to call these material subroutines and analyze the mechanical properties of the structure through data exchange between them.

The function of UMAT is mainly to calculate the Jacobian matrix and the corresponding stress and strain and to update other state variables. The main program of ABAQUS will form a stiffness matrix according to the Jacobian matrix in UMAT and then solve the

response of the structure, including the displacement and strain increment, and UMAT will update the state of the structure according to these variables.

The solving steps of UMAT based on the fatigue damage model in Section 2 are shown in Fig. 8. The subroutine consists of a matrix of four state variables STATEV, which are used to save some user-defined variables. STATEV(1) is used to save the stress components of the material in the load-analysis step in each cycle block. STATEV(2) is used to save the stress components in the unloading analysis step in each cycle block. STATEV(3) and (4) are used to save the updated elastic modulus E and damage value D in each cycle block.

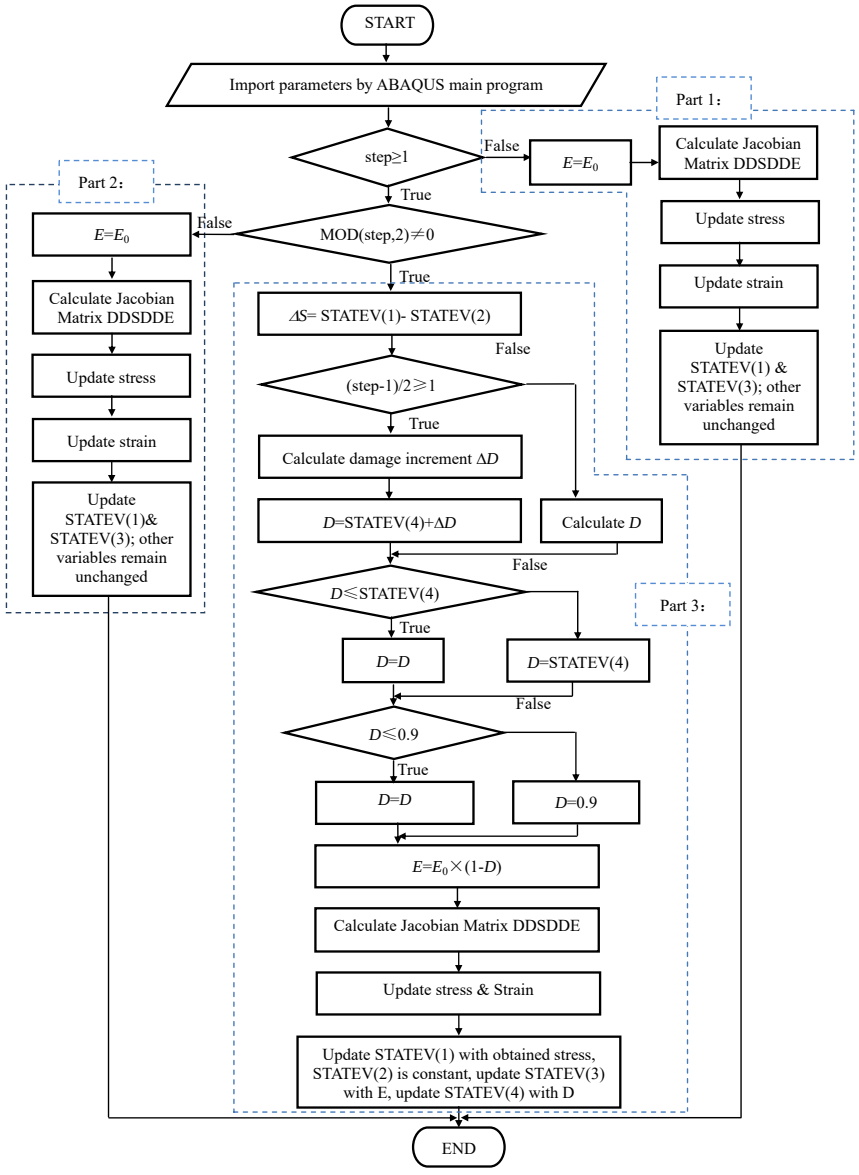

Figure 8: Flow chart of user-defined material subroutine UMAT algorithm

UMAT includes three steps. The first step corresponds to the first loading step when the step is equal to 1. Under this condition, there is no accumulated damage to the material; that is, D is equal to 0, and the elastic modulus is equal to the initial elastic modulus E_0. E_0 is used to generate the Jacobian matrix DDSDDE and calculate the stress and strain. According to the calculation results of the stress and strain, state variables STATEV(1) and STATEV(3) are updated, while other state variables remain unchanged. This analysis step corresponds to the situation of the structure from bearing the maximum load to the minimum load, and thus the structure will not accumulate damage. In other words, the accumulated damage value in the material at this analysis step is the same as in the previous analysis step (loading analysis step); that is, the elastic modulus is equal to the updated elastic modulus in the previous analysis step and is used to generate DDSDDE. The stress and strain are calculated to update the state variable STATEV(2), while the other state variables remain unchanged. The third step corresponds to the loading analysis step when the step is odd and is not equal to 1. The function of this analysis step is to increase the load borne by the structure from the minimum to the maximum. D and the stress value during this loading analysis step are calculated. Before calculating D, it is necessary to calculate the difference between the stress under the loading analysis step and unloading analysis, that is, the stress range ΔS.The obtained ΔS is used to calculate the cumulative damage increment ΔD given in Eq. (9). ΔD is added to D (stored in the state variable STATEV(4)) obtained in the previous cycle block to obtain the accumulated damage value before this loading analysis step. It should be noted that when the cyclic block is equal to 2, D can be directly calculated instead of ΔD, because ΔD generated in the first cycle is the total damage value. After calculating D, it is necessary to verify the damage value to ensure that it is not less than the damage value in the previous cyclic block and not greater than 0.9. Then, the elastic modulus is updated according to the total damage value, and the stress and strain are calculated. Finally, the obtained stress component, E and D are saved in the state variables STATEV(1), (3) and (4).

4.3 Verification of UMAT

To verify the effectiveness of UMAT, the simulation results are compared with the test results of steel wire without initial damage under uniaxial tensile fatigue loads given in the literature [Lan, Xu and Ren (2017)]. The steel wire sample was taken from a segment of finished cable from a cable factory in China and was a high-strength steel wire with a tensile strength of 1670 MPa, length of 250 mm and diameter of 7 mm. During the fatigue test, both ends of the steel wire were clamped for 50 mm, and the length of the standard segment used for analysis was taken as 150 mm. The stress ratio was set at 0.5, and the stress ranges were set as 335 MPa, 418 MPa, 520 MPa and 670 MPa, respectively. The MTS Landmark 100 kN fatigue testing machine was used for the test, and the loading frequency was 10 Hz. The geometry model of high-strength steel wire was established according to the test, as shown in Fig. 9. The density of the model is set as 7.8 g/cm^3, the elastic modulus is 212,000 MPa, and the Poisson's ratio is 0.31 [China National Standardization Management Committee (2008)]. The material subroutine UMAT is used to calculate the fatigue life of the model. The results of numerical simulation are listed in Tab. 1. The test results are compared with the numerical simulation results, as shown in

Fig. 10. The comparison shows that the UMAT written in this paper can achieve the expected goal and that the calculation results are consistent with the experiment results.

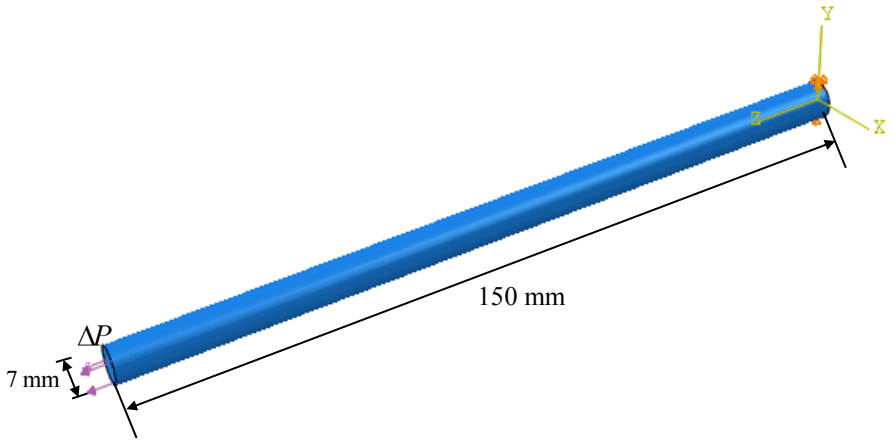

Figure 9: Initial model of steel wire

Table 1: The numerical simulation results by using the UMAT

Stress range /MPa	Accuracy n	Analysis step	Cyclic block	Fatigue life N_f
335	100,000	97	49	4,900,000
418	10,000	223	112	1,120,000
520	10,000	53	27	270,000
670	1,000	97	49	49,000

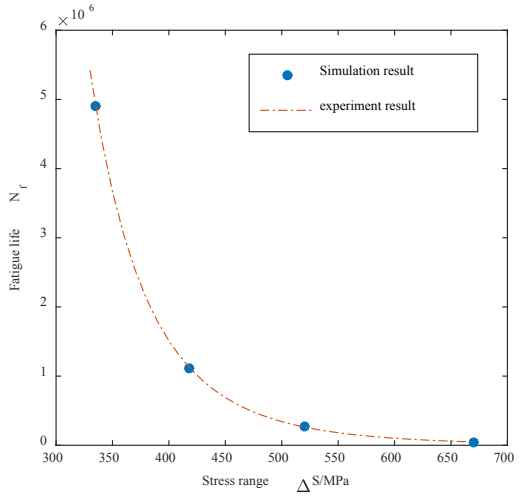

Figure 10: S-N curve of steel wire without the initial defect under uniaxial tensile fatigue load

In addition, since the main object of this paper is to simulate fatigue damage evolution of corroded steel wires, the verification against a structure with defects needs to be made. Therefore, results in the literature [Zheng, Xie, Li et al. (2018)] are adopted to compare with the results from simulation by using UMAT. In the literature [Zheng, Xie, Li et al. (2018)], several fatigue tests of corroded steel wires with a hemispherical pit were conducted and a calculation method based on the damnification tolerance for fatigue life of corroded steel wires was proposed. It is well-known that the relationship between the crack propagation rate da/dN and the stress intensity range ΔK conformed to Paris law is:

$$da/dN = C\Delta K^m \tag{13}$$

where C and m are undetermined parameters that equal 1.39×10^{-12} and 3.3 respectively for steel wire with the diameter of 7 mm when the stress ratio R is 0.5 according to the reference [Zheng, Xie, Li et al. (2018)]. The general formula of ΔK can be expressed as follows:

$$\Delta K = Y\Delta S\sqrt{\pi a} \tag{14}$$

where ΔS is the range of the far-field stress, a is the crack length and Y is the crack shape. The evolutionary equation for the crack shape factor in a notched round-bar specimen is [Zheng, Xie, Li et al. (2018)]:

$$Y = 1.4835 - 2.9219\left(\frac{a}{D}\right) + 5.9602\left(\frac{a}{D}\right)^2 + 1.6304\left(\frac{a}{D}\right)^3 \tag{15}$$

where D is diameter of steel wire and equals 7 mm in this paper.

Therefore, the equation for predicting the crack propagation life can be deduced from Paris law with integral operation:

$$N_f = \frac{1}{C\Delta\sigma^m}\int_{a_0}^{a_c}\left(Y\cdot\sqrt{\pi a}\right)^{-m} da \tag{16}$$

According to the study by Mahmoud [Mahmoud (2007)], the fracture toughness K_{IC} of high-strength steel wire with a diameter of 7 mm is approximately 65.7 $\text{MPa}\cdot\sqrt{\text{m}}$, which is used to calculate the critical length of crack (a_c). The fatigue life of steel wire with a hemispherical pit whose initial diameter is 1 mm (a_0) under different stress ranges is calculated by Eq. (16), as shown in Tab. 2.

Table 2: Fatigue life of steel wire with a hemispherical pit calculated by Eq. (16)

Stress range/MPa	Critical length of crack a_c /mm	Fatigue life N_f
250	2.85	62,203
300	2.43	28,276
350	2.03	13,510
400	1.63	6,034
450	1.26	1,952

According to the fatigue life in Tab. 2, the median S-N curve of steel wire with a hemispherical pit can be expressed as:

$$\lg N_f = 17.45 - 5.202 \times \lg \Delta S \tag{17}$$

The initial geometry model of high-strength steel wire with a hemispherical pit was established according to the test in literature [Zheng, Xie, Li et al. (2018)], as shown in Fig. 11. Other parameters are the same as the model in Fig. 9. The UMAT is used to calculate the fatigue life of the model under different stress ranges. The results of numerical simulation are listed in Tab. 3.

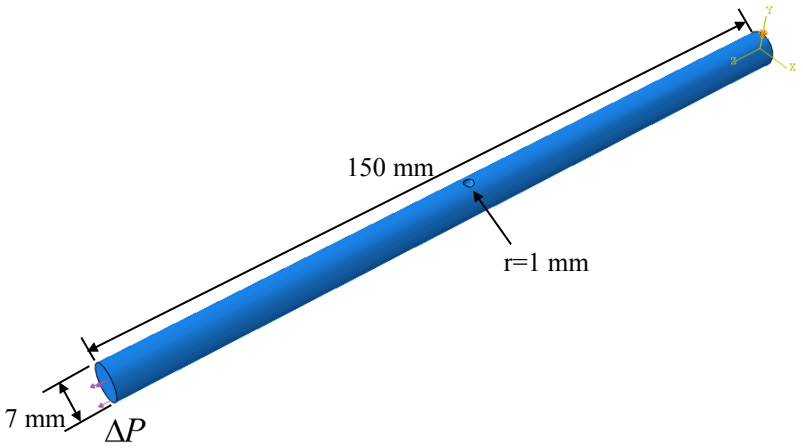

Figure 11: Initial model of steel wire with a hemispherical pit

Table 3: The numerical simulation results by using the UMAT

Stress range ΔS /MPa	Accuracy *n*	Analysis step	Cyclic block	Fatigue life *N*
256	1,000	111	56	56,000
335	500	47	24	12,000
520	100	79	40	4,000

According to the fatigue life in Tab. 3, the median S-N curve of steel wire with a hemispherical pit can be expressed as:

$$\lg N_f = 17.73 - 5.395 \times \lg \Delta S \tag{18}$$

The above two results are compared in Fig. 12. The comparison shows that the UMAT written in this paper can achieve the expected goal and that the calculation results are also consistent well with the results calculated by the damnification tolerance method proposed in the literature [Zheng, Xie, Li et al. (2018)].

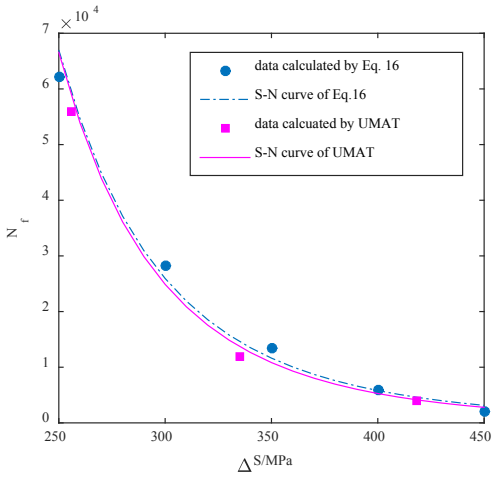

Figure 12: S-N curve of steel wire with a hemispherical pit under uniaxial tensile fatigue load

4.4 Division of the transitional grid and simulation of cyclic loading

To study the corrosion-fatigue damage evolution process of steel wire, this paper examines steel wire with initial defects. The finite element model of the corroded steel wire is established by using the method proposed in Section 2, as shown in Fig. 6. Because of the existence of the initial pit, material failure first appears near the pit, and the damage evolution process mainly occurs around the pit. The initial pit is small, and thus its element size is also small, resulting in a dense grid around the pit. The denser the mesh, the higher the calculation accuracy, but the longer the calculation time. Therefore, a transitional grid is adopted to improve the computational efficiency and effectively reduce the amount of computation, as shown in Fig. 13. To accurately simulate crack propagation, the grid size around the pitting corrosion (z=6 mm~8 mm) is set as 0.1 mm, while the grid size on both sides of the steel wire (z=0mm~4 mm & z=10 mm~14 mm) is set as 0.5 mm, and the grid size between the two areas (z=4 mm~6 mm & 8 mm~10 mm) gradually changes from 0.1 mm to 0.5 mm.

The loading mode of the steel wire specimen mentioned above is uniaxial tensile fatigue load. The stress range of the cyclic load used for simulation in this paper is constant. The applied cyclic load is realized by the script program written in the PYTHON language, and the setting of the cyclic load can be realized efficiently through the script interface of ABAQUS, a commercial finite element software.

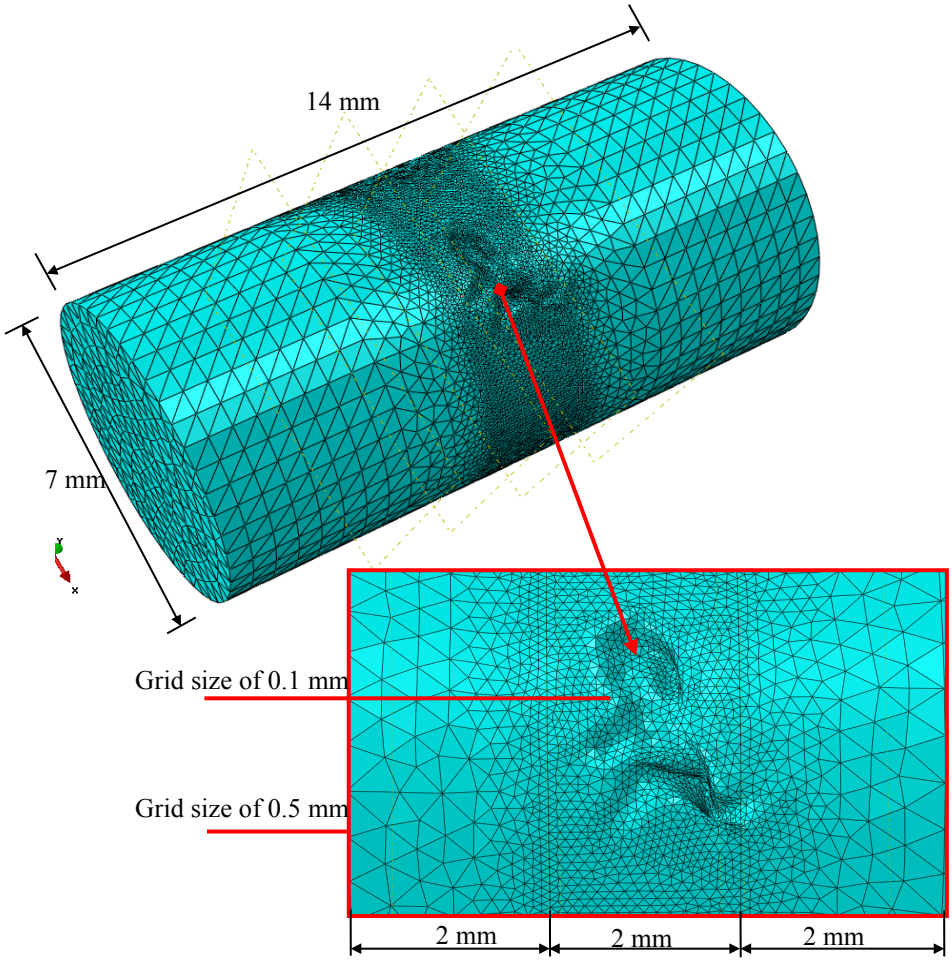

Figure 13: Finite element model of the corroded steel wire

5 Examples

5.1 Study of the damage evolution of steel wire under pre-corrosion fatigue

5.1.1 Initial model and modeling process of corroded steel wire

Based on the method proposed in Section 2, the fatigue damage evolution, fatigue performance and life of corroded steel wire are studied. The mass loss rate η is introduced to evaluate the corrosion degree of corroded steel wire. The expression is as follows:

$$\eta = \frac{m_0 - m_1}{m_0} \times 100\% \tag{19}$$

where m_0 is the initial mass of the wire and m_1 is the mass of corroded steel wire after pickling.

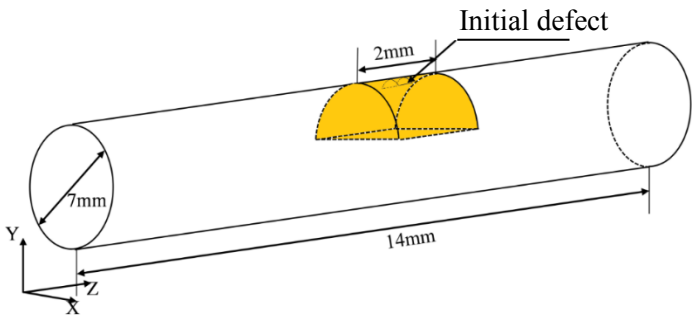

Figure 14: Model and size of corroded steel wire with initial defect

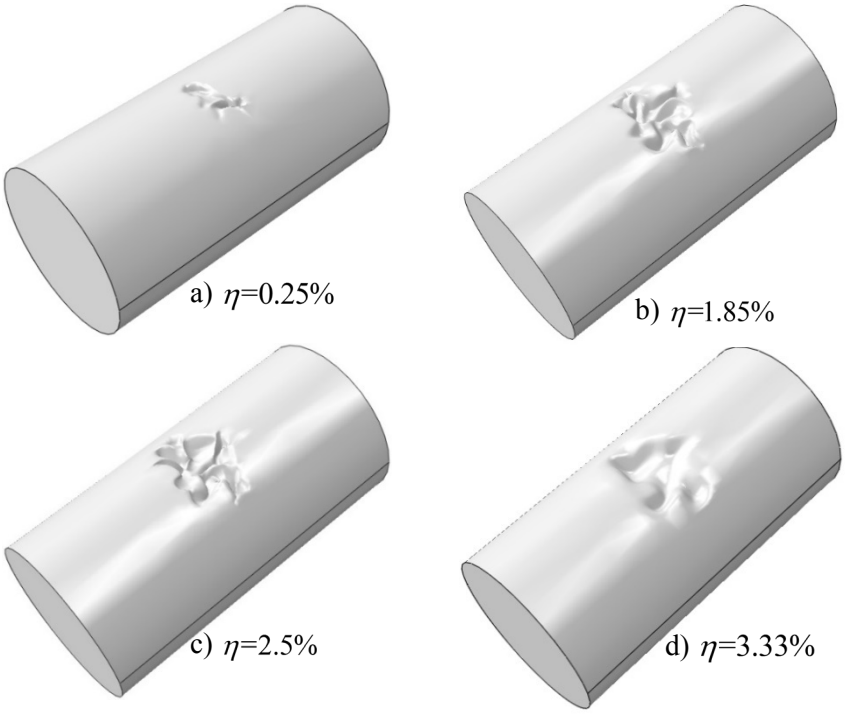

Figure 15: Corroded steel wire model with single pit with different mass loss rates

The accelerated corrosion test was carried out for 1 day, 10 days, 30 days and 60 days. The average mass loss rate of the corroded steel wire was 0.25%, 1.85%, 2.5% and 3.33%, respectively [Lan, Xu and Liu (2018)]. In view of the discrete nature of the pitting test of steel wire, most related studies focus on the fatigue performance of uniformly corroded high-strength steel wire. However, the fracture that often occurs is a pitting defect on the surface of steel wire. Therefore, to achieve the same corrosion degree as the uniform corrosion in the literature [Lan, Xu and Liu (2018)], the upper surface in the middle part of the steel wire is set as the corrosion area in this paper, which means that the initial volume of the steel wire mentioned above is part of the established model, namely, the yellow part in Fig. 14. The size of the initial defect is 0.5 mm*0.5 mm. The modeling method proposed

in Section 3 is used to generate corroded steel wire models with single pit with different mass loss rates, as shown in Fig. 15. The density of the model is set as 7.8 g/cm3, the elastic modulus as 212,000 MPa, and the Poisson's ratio as 0.31 [China National Standardization Management Committee (2008)].

5.1.2 Fatigue life of corroded steel wire

After the initiation of the main crack of the high-strength steel wire, the crack will continue to propagate under the fatigue load. When the stress intensity factor of the crack reaches the fracture toughness, the fracture occurs. This criterion relation can be expressed in the form of Eq. (20) [Fu (1995)]:

$$K_I = Y\sigma\sqrt{\pi x} < K_{IC} \tag{20}$$

where σ is the stress of the specimen and Y is the crack shape factor, which, for a semi-elliptic surface crack under tension on the cylinder, can be expressed as follows [Nakamura and Suzumura (2013)]:

$$Y = \frac{\frac{1.84}{\pi}\left[\tan\left(\frac{\pi x}{2D_i}\right)/\frac{\pi x}{2D_i}\right]^{\frac{1}{2}}}{\cos\left(\frac{\pi x}{2D_i}\right)} \times \left[0.752 + 2.02\frac{x}{D_i} + 0.37\left(1-\sin\left(\frac{\pi x}{2D_i}\right)^3\right)\right] \tag{21}$$

where x is the depth of the pit and D_i is the wire diameter. In this paper, in order to unify the damage assessment system, the stress intensity factor is used to quantify the overall damage degree of high strength steel wire. Therefore, the irregular corrosion pit is equivalent to a semi-elliptic surface crack and do not make too much distinction between the corrosion pit and the crack. Based on the above assumption, the stress intensity factor can be calculated easily by using Eq. (14) and Eq. (15). According to the literature [Mahmoud (2007)], the fracture toughness of high-strength steel wire with a diameter of 7 mm is approximately 65.7 $\text{MPa}\cdot\sqrt{\text{m}}$.

Table 4: Fatigue life of corroded steel wire

Mass loss rate	ΔS /MPa	Accuracy	Cyclic block	x /mm	K_I / $MPa\cdot\sqrt{m}$	Loading numbers	Fatigue life in literature	Error
0.25%	335	100,000	11	0.84906	28.3362	1,100,000		11.36%
			21	0.9873	31.6909	2,100,000	4,304,046	
			31	1.04434	33.0905	3,100,000	3,995,562	
			41	1.46313	43.8541	4,100,000	4,368,983	
			46	2.01576	60.1969	4,600,000	4,213,847	
			47	2.15662	**64.9195**	**4,700,000**	**Ave:4,220,614**	
			48	2.32581	70.9737	4,800,000		
	418	10,000	26	0.83334	34.8836	260,000	1,014,320	6.14%
			51	0.9438	38.2195	510,000	1,205,974	

			76	1.14426	54.0290	760,000	1,105,687	
			96	1.64332	60.9610	960,000	1,048,188	
			98	1.75383	**64.9673**	**980,000**	826,526	
			99	1.79932	66.6611	990,000	**Ave:1,040,139**	
			6	0.90588	46.1171	60,000		
			11	0.90588	46.1171	110,000	232,963	
							246,119	
			16	0.97024	48.5453	160,000	256,961	
	520	10,000					235,852	4.19%
			21	1.15679	55.7050	210,000	116,893	
							325,609	
			23	1.34251	**63.0924**	**230,000**	**Ave:240,066**	
			24	1.48497	68.9913	240,000		
			11	0.92639	30.2075	550,000		
			21	1.5334	45.7729	1,050,000	2,453,711	
			31	1.651	49.0757	1,550,000	2,469,835	
	335	50,000	41	1.71739	50.9955	2,050,000	2,542,617	0.04%
			50	2.15101	**64.7262**	**2,500,000**	2,529,487	
			51	2.21436	66.9362	2,550,000	**Ave:2,498,912**	
			11	1.48492	55.4567	110,000		
			21	1.4978	55.8947	210,000	607,373	
1.85%			31	1.59764	59.3462	310,000	641,078	
	418	10,000	41	1.651	61.2348	410,000	685,124	25.16%
			48	1.75383	**64.9678**	**480,000**	631,859	
			49	1.86178	69.0308	490,000	**Ave:641,358**	
			11	1.14266	55.1548	22,000	167,765	
			31	1.21351	57.9295	62,000	185,080	
	520	2,000	51	1.32309	62.3051	102,000	173,118	36.71%
			55	1.39253	**65.1381**	**110,000**	169,237	
			56	1.45263	67.6320	112,000	**Ave:173,800**	
			31	1.45829	43.7234	620,000	1,381,860	
			61	1.58549	47.2208	1,220,000	1,218,463	
	335	20,000	91	2.124	63.8017	1,820,000	1,293,784	42.53%
			92	2.1464	64.5677	1,840,000	1,325,683	
			93	2.17891	**65.6922**	**1,860,000**	**Ave:1,304,947**	
			16	1.5286	56.9485	160,000	554,096	
			26	1.60166	59.4874	260,000	508,510	
2.5%	418	10,000	36	1.70954	63.3443	360,000	540,250	29.25%
			37	1.70954	**63.3443**	**370,000**	489,166	
			38	1.81019	67.0697	380,000	**Ave:523,005**	
			21	1.04329	51.3242	21,000	132,792	
			51	1.12350	54.4110	51,000	154,328	
	520	1,000	81	1.34156	63.0539	81,000	125,837	27.95%
			86	1.39672	**65.3108**	**86,000**	140,952	

			87	1.41363	66.0094	87,000	65,080 199,342 97,209 **Ave:119,363**	
3.33%	335	10,000	21	1.22206	37.5373	210,000		15.64%
			51	1.45307	43.5826	510,000	875,665	
			81	1.9993	59.6622	810,000	783,086	
			91	2.15517	64.8695	910,000	805,852	
			95	2.15813	**64.9717**	**950,000**	**Ave:821,534**	
			96	2.27421	69.0798	960,000		
	418	10,000	11	1.41614	53.1448	110,000	406,845	7.04%
			21	1.41614	53.1448	210,000	412,214	
			31	1.67105	61.9527	310,000	381,393	
			37	1.71762	**63.6386**	**370,000**	391,646	
			38	1.83608	68.0493	380,000	**Ave:398,024**	
	520	2,000	11	1.17024	56.2302	21,000	102,127	36.90%
			21	1.18407	56.7715	41,000	97,727 119,376	
			31	1.40164	**65.5137**	**61,000**	73,713	
			32	1.42424	66.4490	63,000	90,461 **Ave:96,681**	

Based on the method proposed in Section 4, the corrosion-fatigue damage evolution of steel wire is studied, and the fatigue life of corroded steel wire with different mass loss rates is obtained. The calculation process and results are shown in Tab. 4. Compared with the test results, the fatigue life of corroded steel wire obtained by this method is generally conservative. The error between the simulation and test results increases with the increase in the corrosion degree and the stress range for three reasons: 1. The experimental data in the literature [Lan, Xu and Liu (2018)] comes from uniform corrosion tests. The number and distribution of corrosion pits cannot be controlled, which is not quite consistent with the initial model established in Fig. 15, especially when the corrosion degree is large. 2. The pitting morphology of the initial model generated by cellular automata is also random, and the randomness of the simulation and test increases the error between them. 3. The size of the steel wire model established in this paper is not consistent with that of the test specimen. The length of the steel wire in this paper is 14 mm, while the length of the steel wire in the literature [Lan, Xu and Liu (2018)] is 150 mm. This difference in length leads to error. However, both results are in the same order of magnitude, and the average error is approximately 20.24%, which demonstrates the reliability and practicability of this method in predicting the fatigue life of corroded steel wire.

Fig. 16 shows the S-N curve of high-strength steel wire with different degrees of corrosion. The fatigue performance of steel wire decreases gradually with increasing corrosion degree. Specifically, for steel wire with a mass loss rate of 0.25%, its fatigue life drops by 4.25%, 13.02% and 12.82%, respectively, relative to nondestructive steel wire under each stress range. For steel wire with a mass loss rate of 1.85%, its fatigue life drops by 49.07%, 57.40% and 58.30%, respectively, compared with nondestructive steel wire under each stress range.

For steel wire with a mass loss rate of 2.50%, its fatigue life drops by 62.11%, 67.16% and 67.40%, respectively, relative to nondestructive steel wire under each stress range. For steel wire with a mass loss rate of 3.33%, its fatigue life drops by 80.65%, 67.16% and 76.88%, respectively, relative to nondestructive steel wire under each stress range. These results show that the influence of pitting corrosion on fatigue life is far greater than its influence on mass loss and that stress concentration is the main reason for the attenuation of the fatigue life of the corroded steel wire.

To further analyze the impact of pitting on the fatigue performance of steel wire, the relationship between fatigue life and corrosion degree under different stress ranges is studied, as shown in Fig. 17. When the mass loss rate is less than or equal to 2.50%, the log value of the fatigue life presents a linear decreasing trend with the mass loss rate. Under this condition, an increase of 0.5% in the mass loss rate leads to a decrease of 0.1 in the log of fatigue life, namely, a decrease of approximately 20.57% in the fatigue life. When the mass loss rate is equal to 3.33%, the log value distribution of the fatigue life of steel wire is not obvious. Therefore, more mass loss rates must be analyzed.

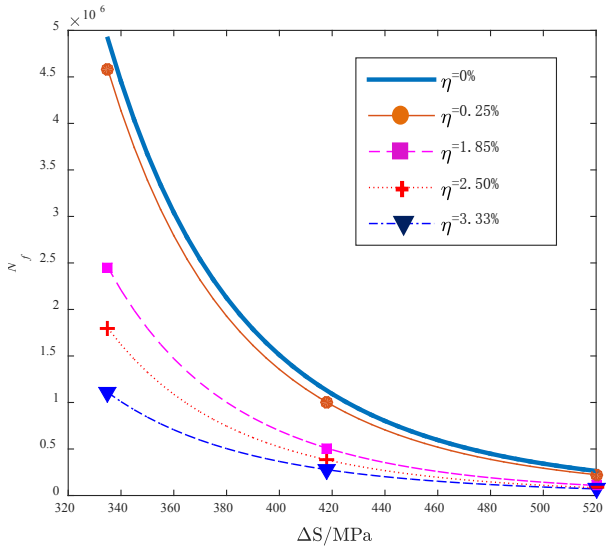

Figure 16: S-N curve of corroded steel wire with different degrees of corrosion

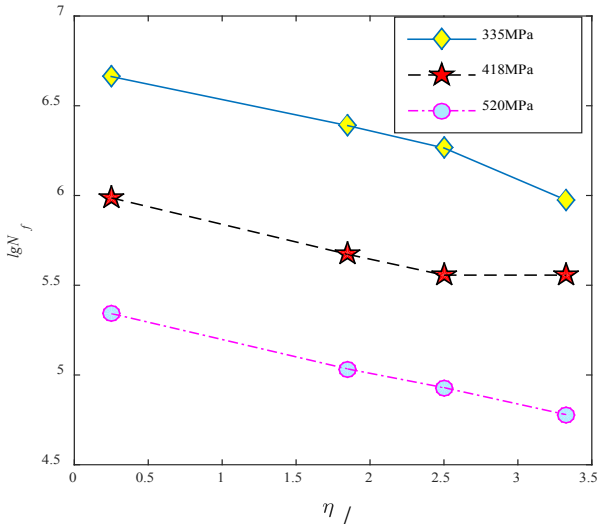

Figure 17: Relationship between corrosion degree and fatigue life

5.1.3 The corrosion-fatigue damage evolution process

To study the change in pitting morphology, the corroded steel wire with a mass loss rate of 0.25% under a stress range of 418 MPa is selected to analyze the corrosion-fatigue damage evolution process. Fig. 18 shows the stress and damage distribution of the steel wire specimen at the 195th analysis step (the loading numbers of 980,000), when it is about to fracture. Fig. 18(a)) shows that the maximum stress appears at the bottom of the pit, and the high stress zone presents a zonal distribution perpendicular to the tension direction. The minimum stress appears at the edge of the pit, and the low-stress zone is distributed along the axis. Fig. 18(b)) shows that the fatigue failure mainly occurs in the high-stress zone and presents a zonal distribution perpendicular to the tension direction, which is affected by the pit morphology.

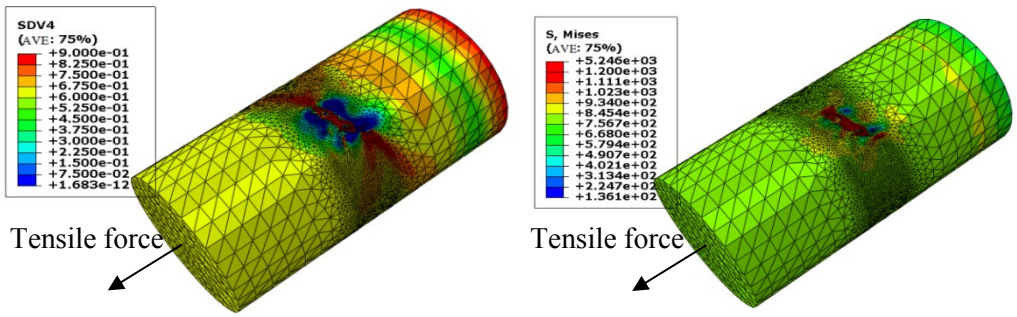

a) Stress contours b) Damage contours

Figure 18: Stress and damage distribution of the corroded steel wire specimen

Fig. 19 shows the damage evolution process and stress distribution on the cross section z=7 mm of the model, in which the left figures present the damaged elements whose color is blue and the right figures present the stress distribution of steel wire. From Fig. 17, the stress concentration occurs in the middle of the pit, where the damage begins to accumulate gradually. As the load continues to increase, damage accumulates and penetrates into the inner zone of the steel wire far from the pit, and the damage evolution rate gradually increases. In addition, the stress distribution in the steel wire changes with the loading process. Due to the stress concentration, the elastic modulus of the material around the pit will gradually attenuate with the cyclic loading; consequently, the deformation energy of the material will change, and its stiffness will decrease. However, under this condition, the damaged material still has the ability to transfer stress and is continuous with the adjacent material, which increases the stress borne by the adjacent materials.

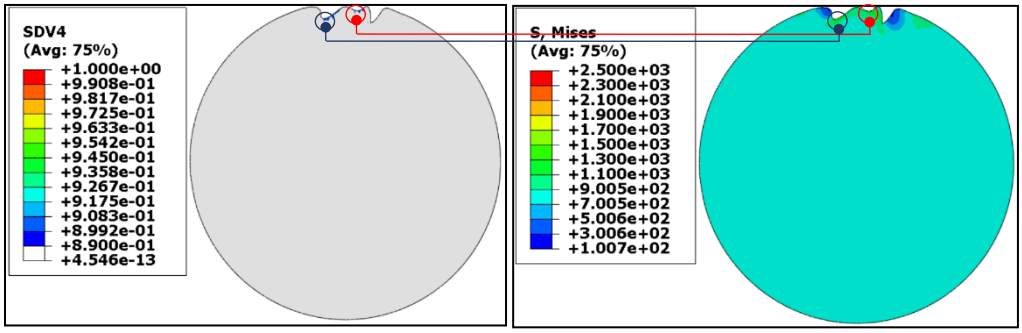

a) 260,000 loading numbers (step=51)

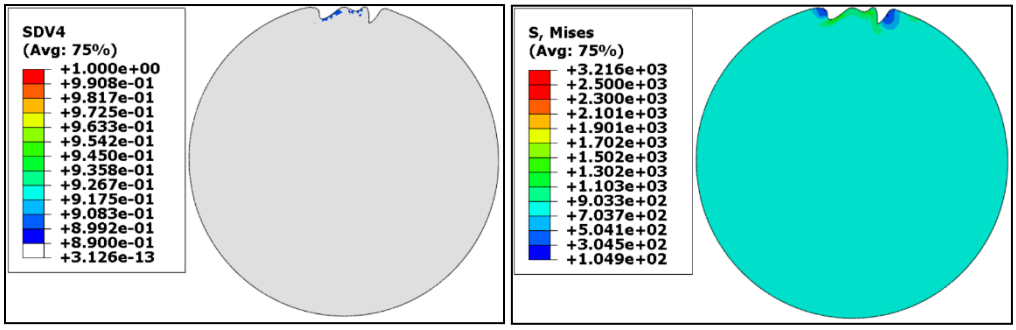

b) 510,000 loading numbers (step=101)

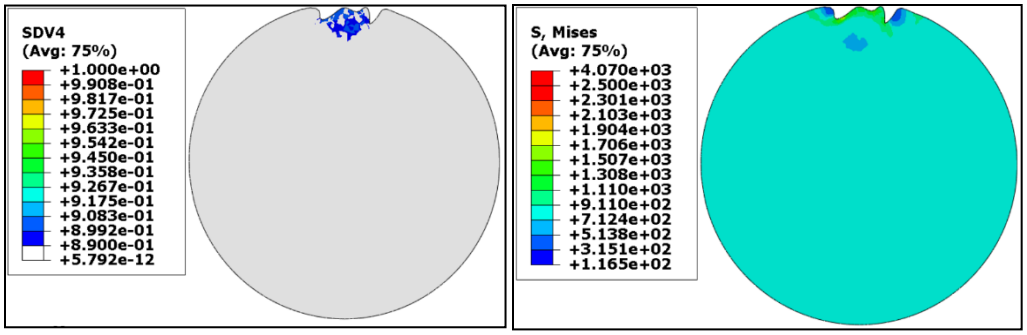

c) 760,000 loading numbers (step=151)

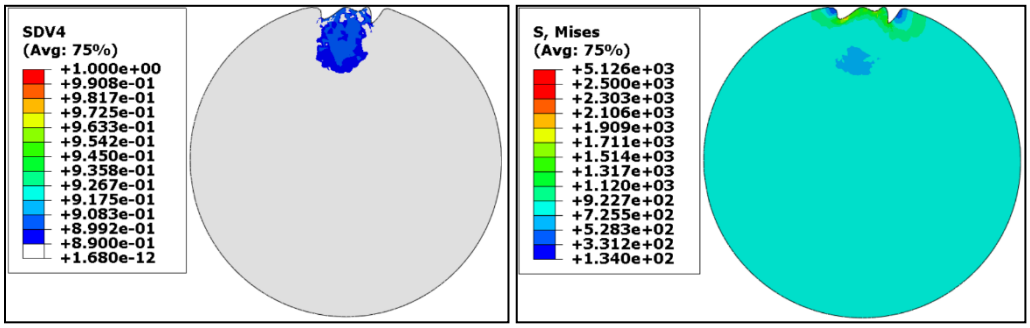

d) 960,000 loading numbers (step=191)

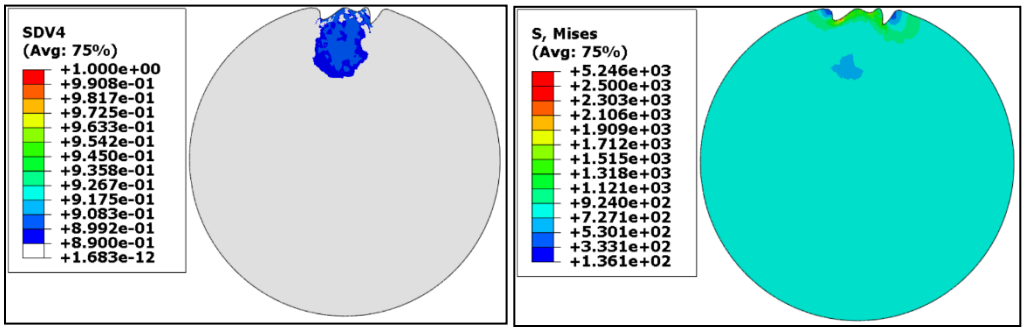

e) 970,000 loading numbers (step=195)

Figure 19: Fatigue damage evolution process and stress distribution of corroded steel wire (z=7)

Fig. 20 presents the time-varying curves of the stress intensity factor and the size of defect. As shown in Fig. 20, with the increase of loading step, the defect size gradually increases, the damage gradually accumulates, and the rate of damage evolution gradually increases. The maximum pit depth is 0.83334, 0.9438, 1.14426 and 1.64332 mm, respectively, at loading numbers of 260000, 510000, 760000 and 960000, and the evolution rates of each loading number interval are $4.4184*10^{-3}$ mm/10,000 cyclic numbers, $8.0184*10^{-3}$ mm/10,000 cyclic numbers and 0.02493 mm/10,000 cyclic numbers, respectively. When

the loading number reaches 980000, the pit depth is 1.75383 mm, and at this moment, the stress intensity factor is 64.9673 $\text{MPa}\cdot\sqrt{\text{m}}$, close to the fracture toughness of 65.7 $\text{MPa}\cdot\sqrt{\text{m}}$, indicating that an instantaneous fracture occurs.

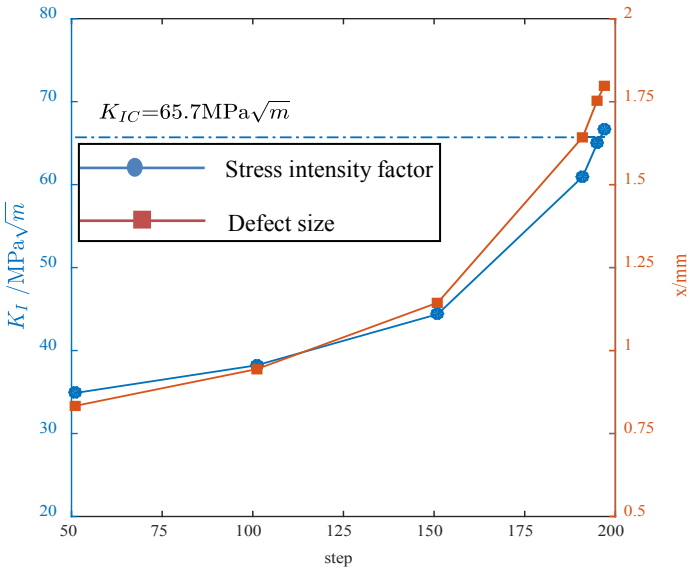

Figure 20: Time-varying curves of the stress intensity factor and the size of defect

5.2 Fracture process of steel wire with multiple fatigue sources

The fractography of corroded steel wire where fatigue fracture occurs can be divided into three zones, namely, crack initiation, crack propagation and instantaneous fracture zones, as shown in Fig. 21 [Zheng, Xie and Li (2017)]. Fig. 21(a) shows that the fatigue crack initiates in a certain pitting defect on the surface, namely, the fatigue source of crack initiation. The crack propagation zone is the zone extending from the center of the fatigue source to the periphery, which appears very smooth after repeated friction under high-frequency fatigue load. The instantaneous fracture zone is the zone where the fracture occurs when the crack propagates to the critical size, which has an irregular stepped shape. There are two fracture types of steel wire with multiple fatigue sources. In one type, crack initiation and propagation are generally in the same plane, as shown in Fig. 21(b). In the other type, crack initiation and are not in the same plane with a stepped fracture, as shown in Fig. 21(c).

Most studies of corrosion-fatigue fracture only focus on the case of a single pit without considering the interaction between multiple pits [Sun (2018); Hu, Meng and Hu (2016)]. To study the fracture process of steel wire with multi-fatigue sources, in this section multiple pits will be set up in the steel wire, and the influence of the number and distribution of pits on the pre-corrosion fatigue life of the steel wire will be studied.

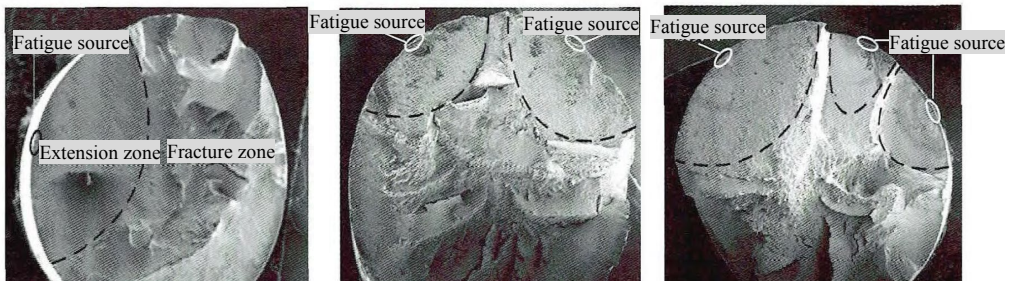

Figure 21: Fractography of corroded steel wire with different fatigue source [Zheng, Xie and Li (2017)]

5.2.1 Steel wire with multiple planar fatigue sources

In this section, five steel wires with different corrosion morphologies are analyzed, as shown in Figs. 22-24. Case 1 is the corrosion steel wire with a single pit. The location of the pit is shown in Fig. 22(a), and the models of the corroded steel wire with corresponding mass loss rates of 1.85% and 3.33% are shown in Fig. 23(a) and Fig. 24(a), respectively. Case 2 is the corroded steel wire containing two pits located in the same radial section, and the angle between the two pits is set to 90°. The locations of the pits are shown in Fig. 22(b), and the models of the corroded steel wire with corresponding mass loss rates of 1.85% and 3.33% are shown in Fig. 23(b) and Fig. 24(b), respectively. Case 3 is the corroded steel wires with three pits in the same radial section, and the angle between adjacent pits is set as 45°. The locations of the pits are shown in Fig. 22(c), and the models of the corroded steel wire with corresponding mass loss rates of 1.85% and 3.33% are shown in Fig. 23(c)) and Fig. 24(c), respectively. Case 4 is also the corroded steel wires with three pits in the same radial section, but the angle between adjacent pits is set as 60°. The locations of the pits are shown in Fig. 22(d), and the models of the corroded steel wire with mass loss rates of 1.85% and 3.33% are shown in Fig. 23(d) and Fig. 24(d), respectively. Case 5 is also the corroded steel wires with three pits in the same radial section, but the angle between adjacent pits is set as 90°. The locations of the pits are shown in Fig. 22(e), and the models of the corroded steel wire with mass loss rates of 1.85% and 3.33% are shown in Fig. 23(e) and Fig. 24(e), respectively. The other parameters are the same as those in Section 5.1.1.

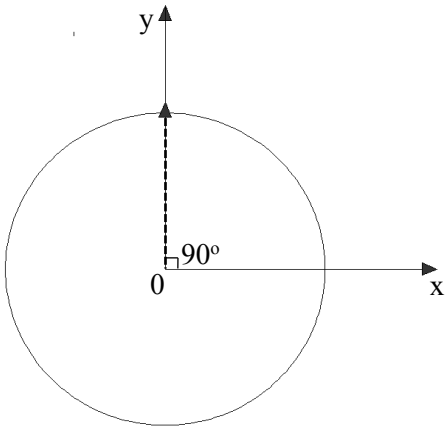

a) Case 1

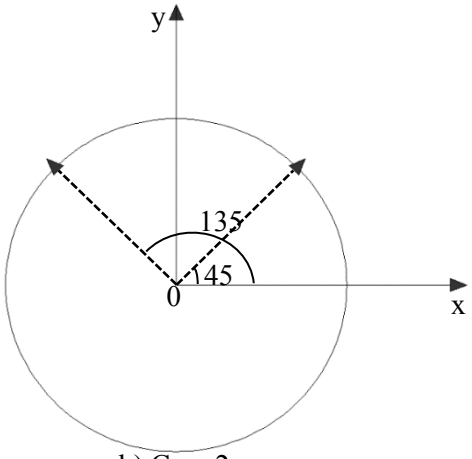

b) Case 2

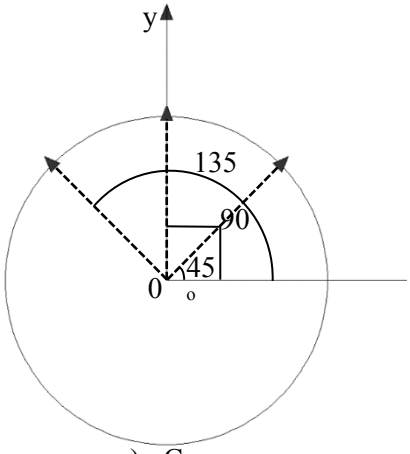

c) Case

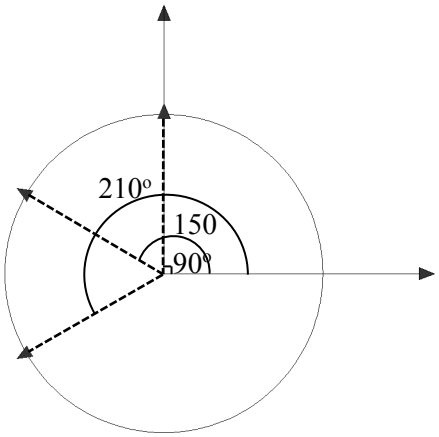

d) Case 4

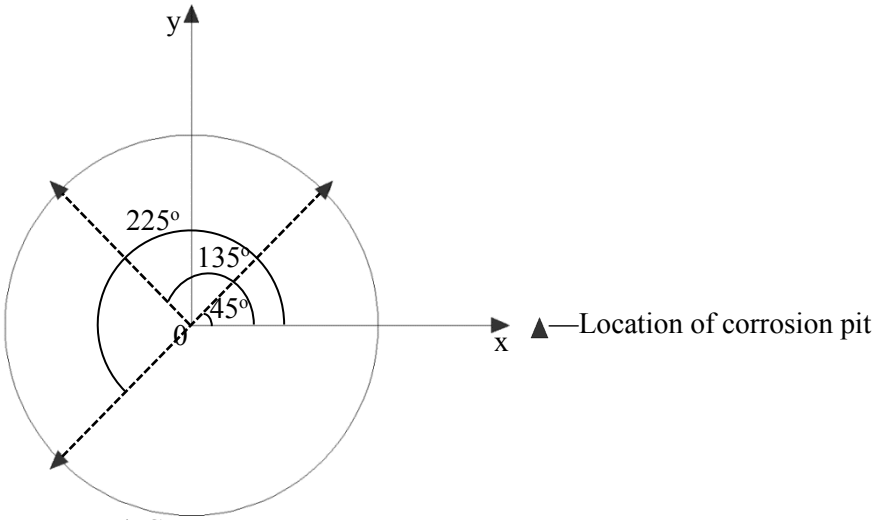

Figure 22: Cross-section diagram of corroded steel wires with different planar multi-fatigue sources (z=7 mm)

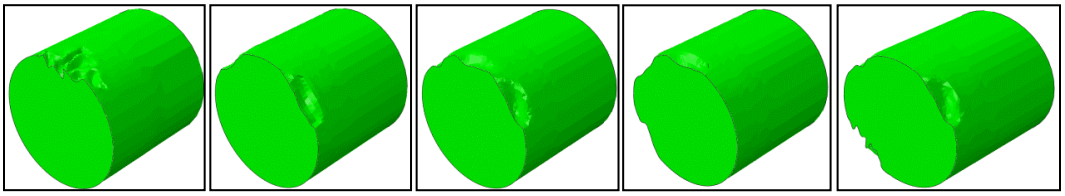

Figure 23: Corroded steel wire models with different planar multi-fatigue sources (η=1.85%)

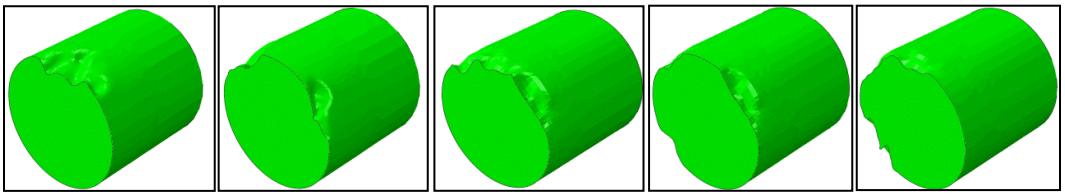

Figure 24: Corroded steel wire models with different planar multi-fatigue sources (η=3.33%)

Material subroutine UMAT is used to calculate the fatigue life of corroded steel wire under a cyclic load with a stress range of 418 MPa. The calculation results are shown in Tab. 5. Whether the mass loss rate is 1.85% or 3.33%, the fatigue life of the corroded steel wire in case 1 is the minimum, while the fatigue life of the corroded steel wire in case 5 is the

maximum. Comparing cases 1, 2 and 5 shows that, under the same mass loss rate and angle of pits, the fatigue life of the corroded steel wire increases gradually with the increase in the number of pits. Fig. 25 is a stress contour of a corroded steel wire with a mass loss rate of 3.33% at the 73rd analysis step (loading number 370,000) in the three cases. As shown in Fig. 25, as the number of pits increases, the depth of pits decreases, which leads to a decrease in the stress concentration in the pit. For example, the maximum stress of steel wire containing a single pit is 1.22 times that of steel wire containing two pits and 1.5 times that of steel wire containing three pits, thus leading to an increase in the fatigue life of the corroded steel wire.

Table 5: Fatigue life of corroded steel wire with different planar fatigue sources

Mass loss rate	Case	Number of pits	Angle between pits	Fatigue life
1.85%	1	1	--	480,000
	2	2	90°	640,000
	3	3	45°	650,000
	4	3	60°	680,000
	5	3	90°	700,000
3.33%	1	1	--	370,000
	2	2	90°	510,000
	3	3	45°	420,000
	4	3	60°	490,000
	5	3	90°	640,000

Note: accuracy: One cycle is equal to two analysis steps and 10,000 loading numbers.

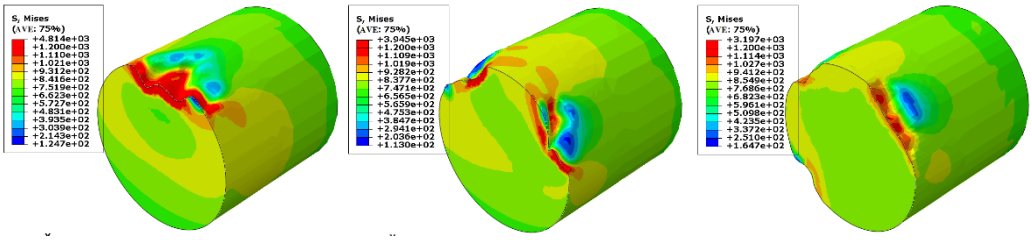

a) Case 1 b) Case 2 c) Case 5

Figure 25: Stress contour of corroded steel wire with different number of pits

Fig. 26 is the time-varying curves of stress intensity factor of corroded steel wires with a mass loss rate of 3.33% in cases 1, 2 and 5. As shown in Fig. 26, the variation trends of these three curves are basically consistent, which indicates that the influence of the number of pits on the damage evolution rate is slight when the angle between adjacent pits equals 90°. Therefore, the main reason for the increase of fatigue life with the increase of the number of pits is the difference between initial damage (the initial pit depth) in different cases.

The points of A, B and C in Fig. 26 are corresponding to the 73rd analysis step. The damage contour of corroded steel wires with a mass loss rate of 3.33% in cases 1, 2 and 5 under this step is shown in Fig. 27(a)). From Fig. 27(a)), the corroded steel wire in case 1 has fractured. At this moment, in cases 2 and 5, the damage degree around the pit with the maximum depth is obviously greater than that of the other pits, but the damage areas around corrosion pits evolve independently and don't mutually affect. The points of D and E in Fig. 26 are corresponding to the 101st analysis step. The damage contour of corroded steel wires with a mass loss rate of 3.33% in cases 2 and 5 under this step is shown in Fig. 27(b)). From Fig. 27(b)), the corroded steel wire in case 2 has also fractured. Under this condition, the damage areas of the two pits are connected. For the corroded steel wire in case 5, the damage areas gradually expand, and the damage areas around the two pits are connected to each other. The point of F in Fig. 26 is corresponding to the 127th analysis step. The damage contour of corroded steel wires with a mass loss rate of 3.33% in case 5 under this step is shown in Fig. 27(c)). From Fig. 27(c)), the damaged areas of the three pits on the section of the corroded steel wire are connected to each other, and the steel wire breaks. The results show that in the process of planar multi-fatigue source fracture, damage usually appears in one pit with a relatively high degree of corrosion, and in the process of damage evolution, the damage areas near each fatigue source gradually connect with each other, eventually leading to fatigue failure of the steel wire specimen.

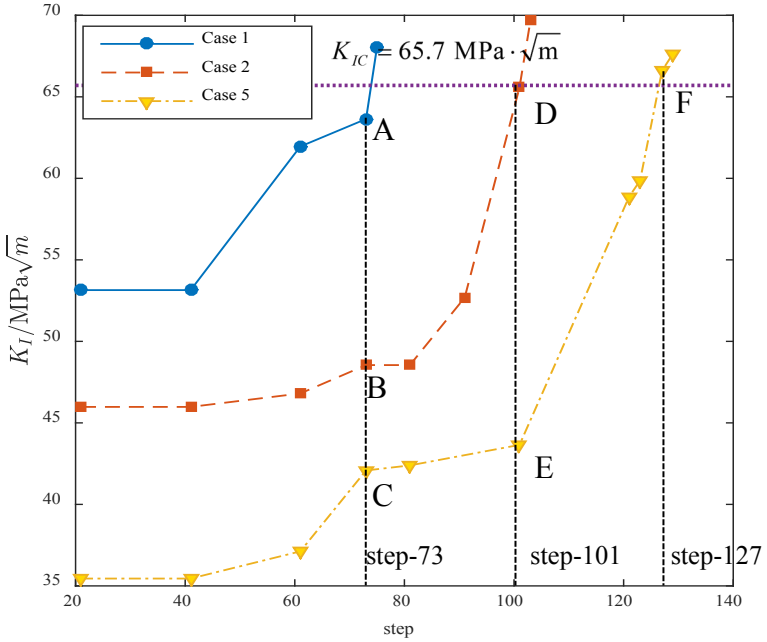

Figure 26: Time-varying curves of the stress intensity factor of steel wires corresponding to the cases in Fig. 24

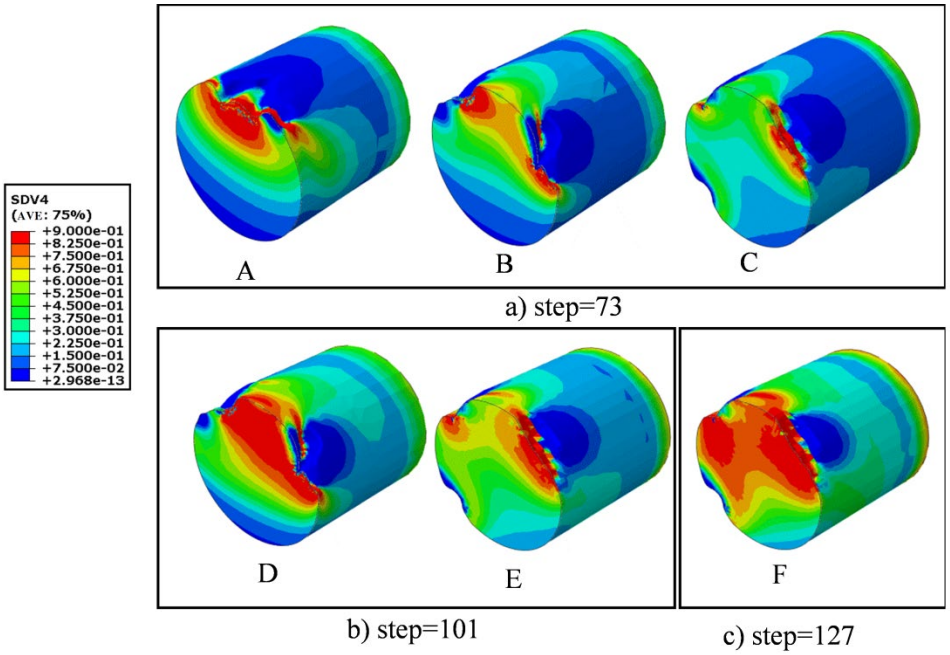

Figure 27: Damage contour of steel wires corresponding to the points in Fig. 26

Comparing cases 3, 4 and 5 shows that, under the same mass loss rate and number of pits, the fatigue life of the corroded steel wire increases gradually with the increase in the angle between pits. However, the larger the angle of the pits, the higher the stress concentration in the pits, and the larger the maximum stress value, which is often unfavorable for the fatigue performance of corroded steel wire, as shown in Fig. 28. The mass rates of steel wires in Fig. 28 are 1.85%.

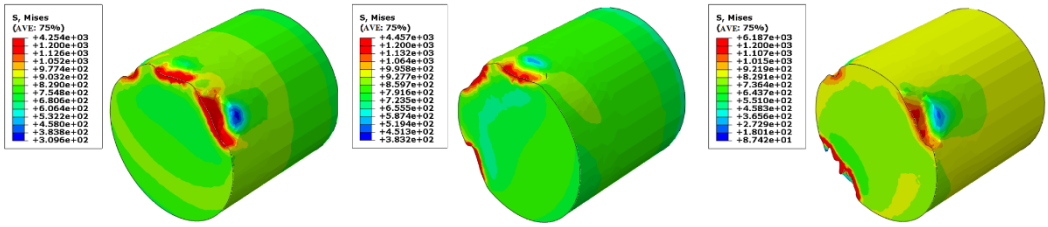

Figure 28: Stress contour of corroded steel wire with different number of pits

Fig. 29 is the time-varying curves of stress intensity factor of corroded steel wires with a mass loss rate of 1.85% in cases 3, 4 and 5. As shown in Fig. 29, the damage evolution rate of the steel wire in case 3 is significantly higher than that in cases 4 and 5. So even if the initial damage of the steel wire in case 3 is less than that in other two cases, which is caused by the random distribution of pitting defects, the fatigue life in case 3 is the lowest among the three cases.

The points of A, B and C in Fig. 29 are corresponding to the 129th analysis step. The damage contour of corroded steel wires with a mass loss rate of 1.85% in cases 3, 4 and 5 under this step is shown in Fig. 30. From Fig. 30, the damage areas around three pits in cases 3 and 4 have connected, which indicates that the steel wires have fractured or are going to fracture; while for the steel wire in case 5, the damage areas around the pits are still independent mutually, and the fracture of the steel wire need the further loading.

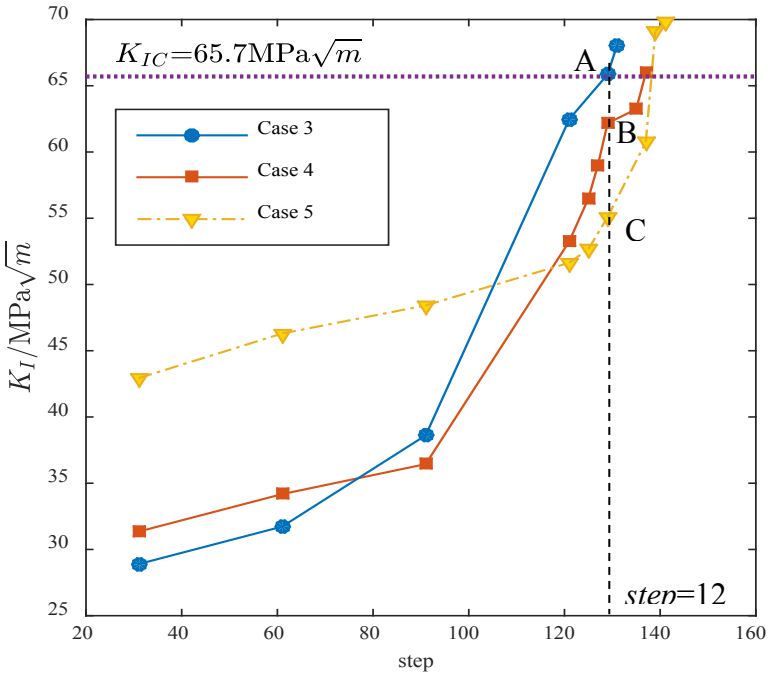

Figure 29: Time-varying curves of the stress intensity factor of steel wires corresponding to the cases in Fig. 23

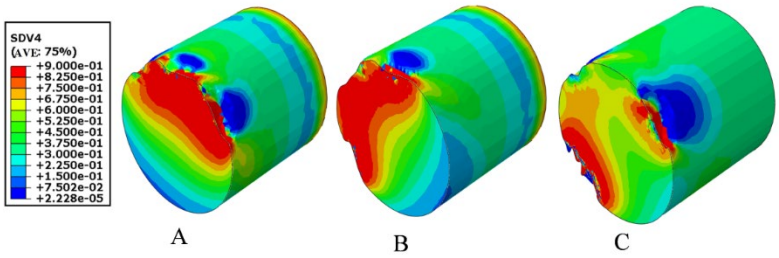

Figure 30: Damage contour of steel wires corresponding to the points in Fig. 29

5.2.2 Steel wire with stepped multi-fatigue sources

In this section, four steel wires with different corrosion morphologies are studied, as shown in Fig. 31, Fig. 32 and Fig. 33. Case 1 is the corroded steel wire with a single pit. The

location of the pit in this case is shown in Fig. 31(a)), and the corresponding mass loss rates are 1.85% and 3.33%, respectively, as shown in Fig. 29(a) and Fig. 33(a). Case 2 is the corroded steel wire with two pits, which are located in different sections and 2 mm apart along the length direction of the wire. The locations of the pits in this case are shown in Fig. 31(b)), and the corresponding mass loss rates of 1.85% and 3.33% are shown in Fig. 32(b)) and Fig. 33(b), respectively. Case 3 is the steel wire with two pits, which are 4 mm apart along the length direction of the wire. The locations of the pits in this case are shown in Fig. 31(c), and the corresponding mass loss rates of 1.85% and 3.33% are shown in Fig. 32c) and Fig. 33(c), respectively. Case 4 is the steel wire with three pits, which are located in different sections, and the distance d between adjacent pits is set as 2 mm. The locations of the pits in this case are shown in Fig. 31(d), and the corresponding mass loss rates of 1.85% and 3.33% are shown in Fig. 32(d) and Fig. 33(d), respectively.

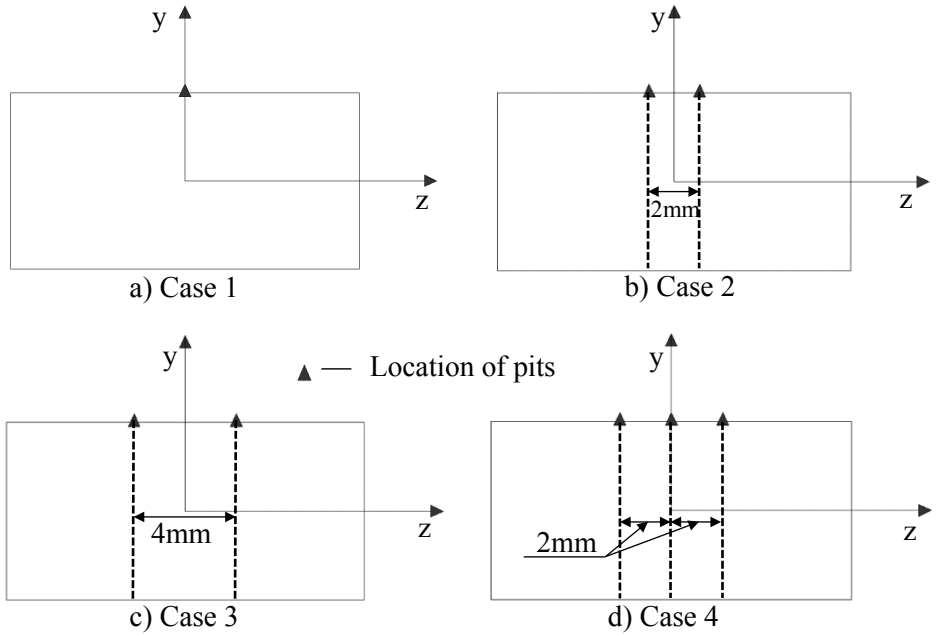

Figure 31: Cross sections of corroded steel wire with different stepped multi-fatigue sources (x=0 mm)

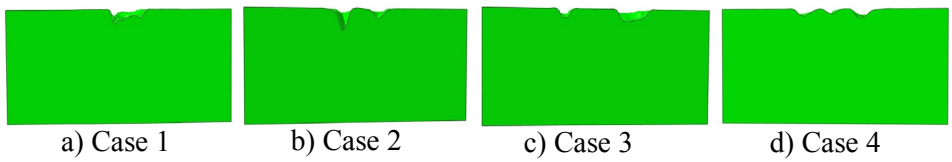

Figure 32: Corroded steel wire model with different stepped multi-fatigue sources (η=1.85%)

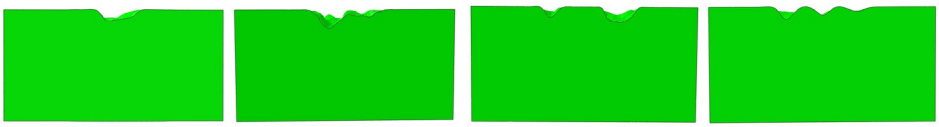

a) Case 1 b) Case 2 c) Case 3 d) Case 4

Figure 33: Corroded steel wire model with different stepped multi-fatigue sources (η=3.33%)

The user-defined material subroutine UMAT is used to calculate the fatigue life of the corroded steel wire under the cyclic load with a stress range of 418 MPa. The method of calculation of the fatigue life is the same as in Section 5.1.2, and the calculation results are shown in Tab. 6. Regardless of whether the mass loss caused by pre-corrosion is large or small, the fatigue life of the corroded steel wire is lowest in case 1, while the fatigue life is highest in case 4. Specifically, when the mass loss rate and the distance of the pits are the same, the fatigue life of the corroded steel wire is proportional to the number of pits. Obviously this result is related to the depth of the pit and is the same as the conclusion reached for the steel wire with a planar multi-fatigue source. For example, as shown in Fig. 34, when the mass loss rate is 1.85% and the analysis step is 95, the maximum depth of the pit under case 1 is 1.428 mm, which is 1.2 times and 2.3 times those under cases 2 and 3, respectively. As a result, the maximum stress in case 1 is 1.5 times and 2.62 times those in cases 2 and 3, and the fatigue performance of the corroded steel wire in case 1 is lower than those under cases 2 and 3.

Table 6: Fatigue life of corroded steel wire with different stepped multiple-fatigue sources

Mass loss rate	Case	Number of pits	Distance between pits	Fatigue life
1.85%	1	1	--	480,000
	2	2	2 mm	520,000
	3	2	4 mm	730,000
	4	3	2 mm	830,000
3.33%	1	1	--	370,000
	2	2	2 mm	440,000
	3	2	4 mm	540,000
	4	3	2 mm	740,000

Note: accuracy: One cycle is equal to two analysis steps and 10,000 loading numbers.

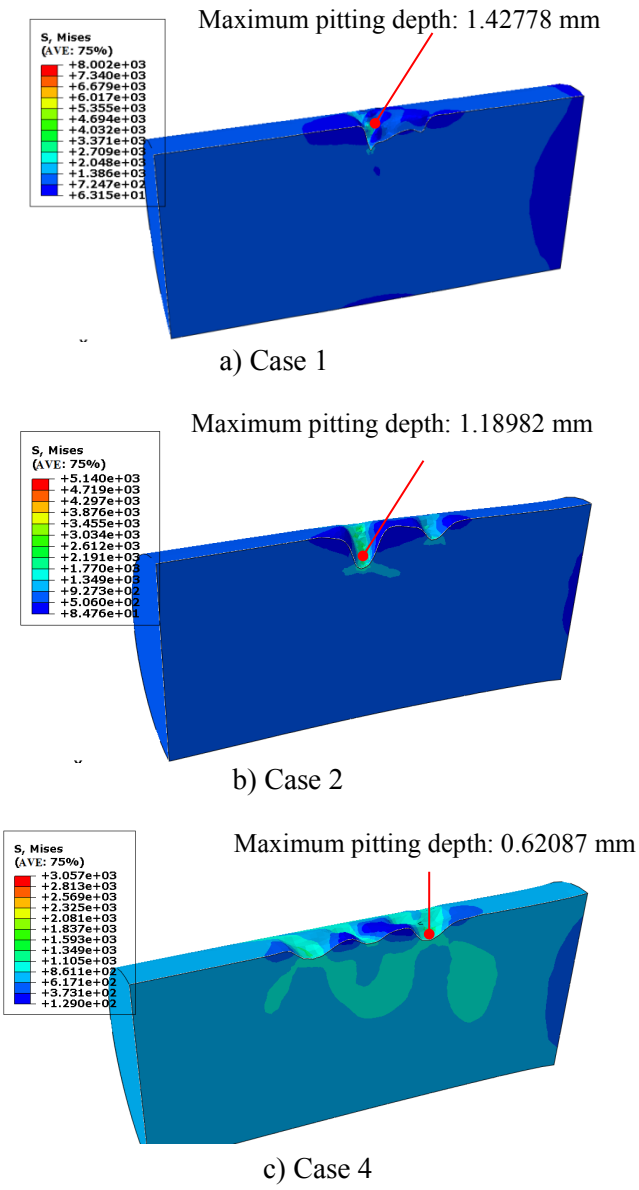

Figure 34: Stress contour of corroded steel wire with number of corrosion pits

Fig. 35 is the time-varying curves of stress intensity factor of corroded steel wires with a mass loss rate of 1.85% in cases 2 and 4. As shown in Fig. 35, the variation trends of these two curves are basically consistent, which indicates that when the distance between pits equals 2 mm, the influence of the number of pits on the damage evolution rate is slight. Therefore, as mentioned above, the main reason for the increase of fatigue life with the increase of the number of pits is the difference between initial damage (the initial pit depth) in different cases.

The points of A, B, C and D in Fig. 35 are corresponding to the 81st, 101st, 151st, 165th analysis step. The damage contour of corroded steel wires with a mass loss rate of 1.85% in cases 2 and 4 under this step is shown in Fig. 36. From Fig. 36, the number of pits has little influence on the fracture of the stepped multi-fatigue source. When multiple pits are distributed along the axial direction, they are independent o each other and the damage areas around the pits evolve independently. When the damage around the pit reaches the critical state of fracture, the steel wire breaks. This process is consistent with the damage evolution of steel wire with a single pit.

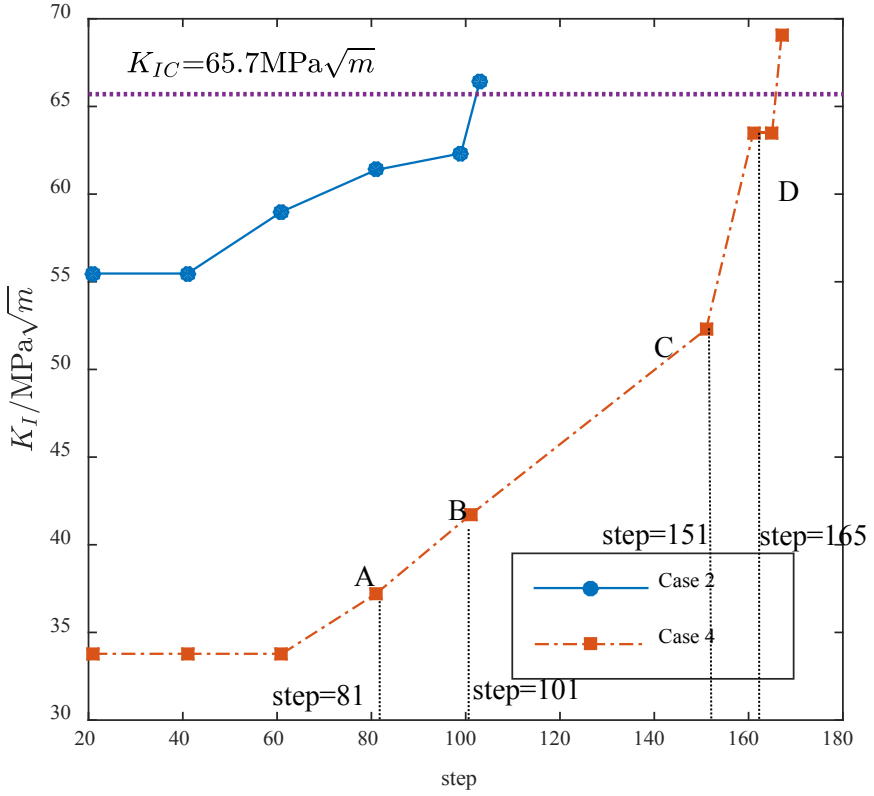

Figure 35: Time-varying curves of the stress intensity factor of steel wires corresponding to the cases in Fig. 31

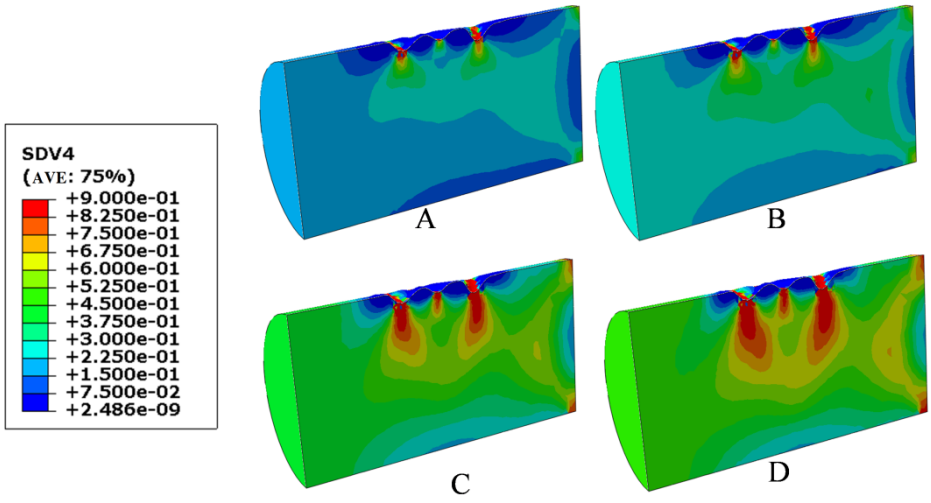

Figure 36: Damage contour of steel wires corresponding to the points in Fig. 35

The comparison of cases 2 and 3 shows that when other conditions are consistent, the larger the distance between pits, the higher the fatigue life of the corroded steel wire. Fig. 37 is the stress contour of the corroded steel wire in cases 2 and 3 (mass loss rates equal to 3.33%). The stress distributions of the two cases are similar. However, as the distance between pits increases, the volume of the low-stress zone increases, and the maximum stress decreases, leading to enhancement of fatigue performance and an increase in the fatigue life of the steel wire.

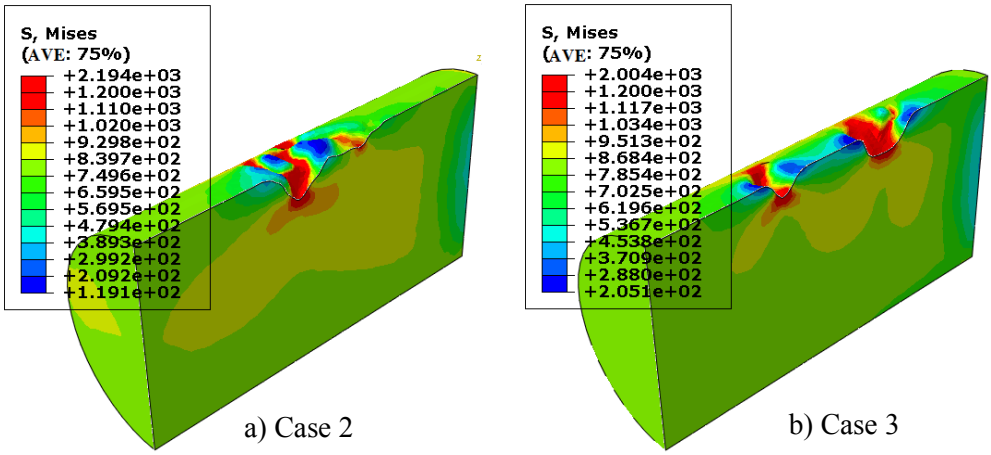

Figure 37: Stress contour of corroded steel wire with stepped multi-fatigue sources

6 Conclusions

1) In this paper, cellular automata (CA) technology is adopted to simulate the damage evolution process of metal corrosion in three-dimensional cellular space. A metal/passive

film/electrolyte system is considered as an automata system with special local rules/transformation rules and discretized into a CA system in an orderly cellular grid to obtain the morphology of metal corrosion pits on the surface and their size and distribution. Then, by using the griddata( ) function to interpolate the generated pitting data and compiling the conversion function, the model can be imported into AutoCAD, Rhino and ABAQUS software in succession to generate the required three-dimensional geometric model of corroded steel wire with irregular pits. The model is based on the mechanism of metal anodic dissolution and can reasonably describe the irregular morphology and distribution of pits in line with the actual situation.

2) A structural solving process based on a cyclic block is presented in this paper, and the solving process of each seemingly independent cyclic block is connected to form a nonlinear analysis process. At the same time, the calculation of damage is mainly related to the cyclic block. The concept of the life-and-death element method is used to control the failure of the element. Based on the fatigue damage model, the user-defined material subroutine is written, which can adequately simulate the material damage evolution and failure process under cyclic loads. The effectiveness of the material subroutine is verified by comparison of the numerical simulation results with the test results for a steel wire specimen without initial defect and with a hemispherical pit under uniaxial tensile conditions.

3) Based on the numerical simulation method proposed in this paper, the pre-corrosion fatigue life of steel wire is calculated. The results show that the fatigue life of the corroded steel wire obtained by this method is generally conservative, especially when the corrosion degree and the stress range are large. However, considering the randomness of simulations and experiments, this method can basically achieve the expected goal and has high reliability and practicability in predicting the fatigue life and simulating the damage evolution of corroded steel wire.

4) Based on the method proposed in this paper, the fatigue life of corroded steel wires with different degrees of corrosion under the action of different stress ranges is calculated. The results show that as the corrosion degree increases, the fatigue performance of steel wire decreases gradually, the effect of pitting corrosion on fatigue life is far greater than the mass loss, and the stress concentration is the main reason for the decline in the fatigue life of pre-corroded steel wire. In addition, when the mass loss rate is relatively small, the log value of fatigue life shows a linear decreasing trend with the mass loss rate. Moreover, the damage evolution process is studied. Under the action of fatigue load, the stress concentration occurs at the bottom of corrosion pit where damage gradually accumulates and penetrates into the inner of steel wire and the damage evolution rate gradually increases.

5) The fracture process of steel wire with multi-fatigue sources and the influence of the number and distribution of pits on the pre-corrosion fatigue life of steel wire are studied. The results show that the planar pitting distribution has a great influence on the damage evolution. The fracture of steel wire with a planar multi-fatigue source is usually caused by one of the pits with high degree of corrosion. When this pit is in the process of damage evolution, the damage areas around it are gradually connected with each other, which eventually leads to the fatigue failure of the steel wire specimen. For the stepped pitting distribution, the pits are independent of each other, and the damage evolution process is consistent with that of the steel wire containing a single pit. The fatigue life of steel wire

is positively correlated with the pitting corrosion number and the angle and distance between pits.

Acknowledgement: The works described in this paper are substantially supported by the grant from the National Natural Science Foundation of China (Grant No. 51678135); the Natural Science Foundation of Jiangsu Province (No. BK20171350); the Fundamental Research Funds for the Central Universities (No. 2242016R30009); the Priority Academic Program Development of Jiangsu Higher Education Institutions (PAPD), the Top-notch Academic Program Project of Jiangsu Higher Education Institutions (TAPP); Six Talent Peak Projects in Jiangsu Province (JNHB-007), which are gratefully acknowledged.

References

Amiri, M.; Arcari, A.; Airoldi, L.; Naderi, M.; Naderi, M. (2015): A continuum damage mechanics model for pit-to-crack transition in AA2024-T3. *Corrosion Science*, vol. 98, pp. 678-687.

Austen, I. M.; Mcintyre, P. (2013): Corrosion fatigue of high-strength steel in low-pressure hydrogen gas. *Metal Science Journal*, vol. 13, no. 7, pp. 420-428.

Chaboche, J. L. (1981): Continuous damage mechanics-a tool to describe phenomena before crack initiation. *Nuclear Engineering and Design*, vol. 64, no. 2, pp. 233-247.

China National Standardization Management Committee (2001): *Corrosion of Metals and Alloys-Evaluation of Pitting Corrosion (GB/T18590-2001)*. Standards Press of China, Beijing (in Chinese).

China National Standardization Management Committee. (2008): *Hot-Dip Galvanized Steel Wires for Bridge Cables (GBT 17101-2008)*. Standards Press of China, Beijing (in Chinese).

Chowdhury, D.; Santen, L.; Schadschneider, A. (2000): Statistical physics of vehicular traffic and some related systems. *Physics Reports*, vol. 329, no. 4, pp. 199-329.

Chen, M. C.; Wen, Q. Q.; Zhu, Q.; Huang, H.; Xie, L. (2017) Simulation of corrosion process for concrete filled steel tubular columns with the cellular automata method. *Engineering Failure Analysis*, vol. 82, pp. 298-307.

DiCaprio, D.; Vautrin-Ul, C.; Stafiej, J.; Saunier, J.; Chausse, A. et al. (2011): Morphology of corroded surfaces Contribution of cellular automata modelling. *Corrosion Science*, vol. 53, no. 1, pp. 418-425.

DiCaprio, D. D.; Vautrin-Ul, C.; Stafiej, J.; Chausse, A.; Feron, D. et al. (2013): Cellular automata approach for morphological evolution of localised corrosion. *British Corrosion Journal*, vol. 46, no. 2, pp. 223-227.

Fu, X. J. (1995): *Structural Fatigue and Fracture*. Northwestern Polytechnical University Press, Xi'an (in Chinese).

Godard, H. P. (2015): The corrosion behavior of aluminum in natural waters. *Canadian Journal of Chemical Engineering*, vol. 38, no. 5, pp. 167-173.

Han, Z. Y.; Huang, X. G.; Cao, Y. G.; Xu, J. Q. (2014). A nonlinear cumulative evolution model for corrosion fatigue damage. *Journal of Zhejiang University Science A*, vol. 15, no. 6, pp. 447-453.

Hirose, Y.; Mura, T. (1985): Crack nucleation and propagation of corrosion fatigue in high-strength steel. *Engineering Fracture Mechanics*, vol. 22, no. 5, pp. 859-870.

Hu, P.; Meng, Q.; Hu, W.; Shen, F.; Zhan, Z. X. et al. (2016): A continuum damage mechanics approach coupled with an improved pit evolution model for the corrosion fatigue of aluminum alloy. *Corrosion Science*, vol. 113, pp. 78-90.

Huang, X. G.; Xu, J. Q. (2012): Pit morphology characterization and corrosion fatigue crack nucleation analysis based on energy principle. *Fatigue & Fracture of Engineering Materials & Structures*, vol. 35, no. 7, pp. 606-613.

Lan, C. M.; Xu, Y.; Liu, C. P.; Li, H.; Spencer, B. F. (2018): Fatigue life prediction for parallel-wire stay cables considering corrosion effects. *International Journal of Fatigue*, vol. 114, pp. 81-91.

Lan, C. M.; Xu, Y.; Ren, D. L.; Li, N.; Liu, Z. Q. (2017): Fatigue property assessment of parallel wire stay cable I: fatigue life model for wire. *China Civil Engineering Journal*, vol. 50, no. 6, pp. 66-74 (in Chinese).

Langton, C. G. (1984): Self-reproduction in cellular automata in physica 10D. *Physica D-Nonlinear Phenomena*, vol. 10. no. 1, pp. 135-144.

Li, X. L.; Song, X. H.; Liu, Y. X. (1995): Investigation on fatigue reliability of high strength galvanized steel wire. *China Civil Engineering Journal*, vol. 2, pp. 36-43 (in Chinese).

Liao, C. M.; Wei, R. P. (1999): Galvanic coupling of model alloys to aluminum-a foundation for understanding particle-induced pitting in aluminum alloys. *Electrochimica Acta*, vol. 45, no. 6, pp. 881-888.

Li, W.; Packard, N. H.; Langton, C. G. (1990): Transition phenomena in cellular automata rule space. *Physica D*, vol. 45, no. 1-3, pp. 77-94.

Mahmoud, K. M. (2007): Fracture strength for a high strength steel bridge cable wire with a surface crack. *Theoretical & Applied Fracture Mechanics*, vol. 48, no. 2, pp. 152-160.

Nakamura, S.; Suzumura, K. (2013): Experimental study on fatigue strength of corroded bridge wires. *Journal of Bridge Engineering*, vol. 18, no. 3, pp. 200-209.

Perkins, K. M.; Bache, M. R. (2005): Corrosion fatigue of a 12%Cr low pressure turbine blade steel in simulated service environments. *International Journal of Fatigue*, vol. 27, no. 10, pp. 1499-1508.

Pidaparti, R. M.; Palakal, M. J.; Fang, L. (2004): Cellular automation approach to model aircraft corrosion pit damage growth. *AIAA Journal*, vol. 42, no. 12, pp. 2562-2569.

Pidaparti, R. M.; Fang, L.; Palakal, M. J. (2008): Computational simulation of multi-pit corrosion process in materials. *Computational Materials Science*, vol. 41, no. 3, pp. 255-265.

Stafiej, J.; DiCaprio, D.; Bartosik, L. (2013): Corrosion-passivation processes in a cellular automata based simulation study. *Journal of Supercomputing*, vol. 65, no. 2, pp. 697-709.

Sun, B. (2018): A continuum model for damage evolution simulation of the high strength bridge wires due to corrosion fatigue. *Journal of Constructional Steel Research*, vol. 146, pp. 76-83.

Watson, S. C.; Stafford, D. (1988): Cables in trouble. *Civil Engineering-ASCE*, vol. 58, no. 4, pp. 38-41.

Wang, H.; Song, B. F.; Wang, L.; Lu, G. Z.; Cui, W. M. (2009): Three-dimensional computational simulation of corrosion pit growth morphology. *Acta Aeronautica Et Astronautica Sinica*, vol. 30, no. 11, pp. 2185-2192 (in Chinese).

Wei, R. P. (2010): Environmental considerations for fatigue cracking. *Fatigue & Fracture of Engineering Materials & Structures*, vol. 25, no. 8-9, pp. 845-854.

Wimpenny, J. W. T.; Colasanti, R. (1997): A unifying hypothesis for the structure of microbial biofilms based on cellular automata models. *FEMS Microbiology Ecology*, vol. 22, no. 1, pp. 1-16.

Yu, S. W. (1988): Fracture damage and microscopic mechanics. *Mechanics in Engineering*, vol. 10, no. 6, pp. 12-18 (in Chinese).

Zheng, X. L.; Xie, X.; Li, X. Z.; Hu, J. M.; Sun, W. Z. (2017): Fatigue fracture surface analysis and fatigue life estimation of corroded steel wires. *China Journal of Highway and Transport*, vol. 30, no. 4, pp. 79-86 (in Chinese).